# Protein Interactome of the Cancerous Inhibitor of Protein Phosphatase 2A (CIP2A) in Th17 Cells

**Mohd Moin Khan [1,2#], Tommi Välikangas [1,3#], Meraj Hasan Khan[1#], Robert Moulder[1], Ubaid Ullah[1], Santosh Dilip Bhosale [1], Elina Komsi[1], Umar Butt[1], Xi Qiao[1], Jukka Westermarck [1,4], Laura L Elo [1] and Riitta Lahesmaa[1*]**

[1]Turku Bioscience Centre, University of Turku and Åbo Akademi University, FI-20520 Turku, Finland.

[2]Turku Doctoral Programme of Molecular Medicine (TuDMM), Medical Faculty, University of Turku, Turku, Finland.

[3] Doctoral Programme in Mathematics and Computer Sciences (MATTI), University of Turku, Turku, Finland

[4] Institute of Biomedicine, University of Turku, Turku, Finland

[#] These authors contributed equally to this work

***Correspondence**

Professor Riitta Lahesmaa

Turku Bioscience Centre,

Tykistökatu 6A (7th floor)

Turku 20520, FINLAND

Phone: 00358-29-4502415

Email: rilahes@utu.fi

**Running Title: Insights of CIP2A Protein Interactome**

## ABSTRACT

Cancerous inhibitor of protein phosphatase 2A (CIP2A) is involved in immune response, cancer progression, and in Alzheimer´s disease. However, an understanding of the mechanistic basis of its function in this wide spectrum of physiological and pathological processes is limited due to its poorly characterized interaction networks. Here we present the first systematic characterization of the CIP2A interactome by affinity-purification mass spectrometry combined with validation by selected reaction monitoring targeted mass spectrometry (SRM-MS) analysis in Th17 cells. In addition to the known regulatory subunit of protein phosphatase PP2A, the catalytic subunit of protein PP2A was found to be interacting with CIP2A. Furthermore, the regulatory (PPP1R18, and PPP1R12A) and catalytic (PPP1CA) subunits of phosphatase PP1 were identified among the top novel CIP2A interactors. Evaluation of the ontologies associated with the proteins in this interactome revealed that they were linked with RNA metabolic processing and splicing, protein traffic, cytoskeleton regulation and ubiquitin-mediated protein degradation processes. Taken together, this network of protein-protein interactions will be important for understanding and further exploring the biological processes and mechanisms regulated by CIP2A both in physiological and pathological conditions.



**Key words:** CIP2A, Interactome, Mass Spectrometry (MS), Selected Reaction Monitoring (SRM) targeted mass spectrometry, confocal microscopy, Pathway analysis.


**Highlights:**

- The first characterisation of the CIP2A interactome in Th17 cells.

- Key interactions were validated by targeted SRM-MS proteomics, western blot and confocal microscopy.
- Pathway analysis of the interactome revealed interrelationships with proteins across a broad range of processes, in particular associated with mRNA processing.

72 **INTRODUCTION**

73 PP2A is a recognized tumor suppressor that imparts crucial functions in regulating cell
74 proliferation, differentiation, and apoptosis [1] – [7] . Accordingly, down regulation of
75 PP2A has been observed as a feature in many cancers. Cancerous Inhibitor of PP2A
76 (CIP2A) was first characterized as an endogenous inhibitor of protein phosphatase 2A
77 (PP2A) in cancer cells [8] . Previous studies have shown that many of the known
78 actions of CIP2A are mediated through inhibition of PP2A [9] , [10] . Overexpression
79 of CIP2A has been associated with the poor prognosis in several human malignancies,
80 and CIP2A has thus been seen as a potential therapeutic target for cancer therapy [8]
81 , [11] , [12] . CIP2A supports the activity of many critical onco-proteins (Akt, MYC,
82 E2F1) and promotes malignancy in most cancer types via PP2A inhibition [8] .
83 Structurally, CIP2A forms a homodimer and this dimerization promotes its interaction
84 with the PP2A regulatory subunits B56$\alpha$ and B56$\gamma$ [13] . Interestingly, inhibition of
85 either CIP2A dimerization or B56$\alpha/\gamma$ expression destabilizes CIP2A in cancer cells
86 [13] . In Alzheimer's disease (AD), enhanced expression of CIP2A in AD brains and
87 neurons results in PP2A inhibition and tau protein hyperphosphorylation, which leads
88 to abnormal tau localization with memory deficits and other pathological conditions
89 [14] .

90 Th17 cells are found at mucosal surfaces where they regulate tissue homeostasis [15]
91 – [18] . Dysregulation of Th17 cell differentiation, however, has been associated with
92 a number of autoimmune inflammatory diseases [19] , [20] . Following our earlier
93 report on the involvement of CIP2A in T cell activation [21] , we subsequently
94 observed that CIP2A negatively regulates T helper (Th)17 cell differentiation, whereby
95 CIP2A depletion resulted in enhanced IL17 expression both in human and mouse

96 Th17 cells (Khan M.M et al., submitted).Thus, CIP2A could have important implications
97 in the differentiation and regulation of Th17 cells. Although CIP2A has been shown to
98 regulate a range of pathological and physiological conditions, there has not been any
99 systematic analysis of the full range of signaling pathways and processes regulated
100 by CIP2A.

101 In the current study, we used immunoprecipitation followed by label free quantitative
102 proteomics to gain insight into the proteins that are associated with CIP2A. We present
103 the first interactome of CIP2A, with validation of interactors by selected reaction
104 monitoring (SRM) targeted mass spectrometry as well as by Western blotting and
105 confocal microscopy. In addition to its known interaction with the regulatory subunit A
106 and B of phosphatase PP2A, our data demonstrated CIP2A interaction with the PP2A
107 catalytic subunits namely PPP2CA and PPP2CB. Furthermore, both the regulatory
108 (PPP1R18, and PPP1R12A) and catalytic (PPP1CA) subunits of phosphatase PP1
109 were identified among the top interactors of CIP2A. This data further implicates the
110 involvement of CIP2A in a number of biological processes that it has previously not
111 been associated to, and provides a basis for comprehensive understanding of CIP2A
112 for translational studies targeting CIP2A in human diseases.

113

## RESULTS

### Mass spectrometry analysis identify novel CIP2A binding partners

To identify the proteins interacting with CIP2A and thereby facilitate the understanding of its functions in human Th17 cells, immunoprecipitation (IP) was performed after 72 h of polarization of naïve T cells towards the Th17 lineage **(Fig. 1A; S1A-C).** The cell model for the study was rationalized by our recent findings indicating that CIP2A is involved in T-cell activation [21] and its particular importance for Th17 cell differentiation (Khan MM et al., submitted). Two CIP2A specific antibodies (Ab1 and Ab2) recognizing distinct regions of CIP2A were used in two biological replicates, together with their respective IgGs (IgG1 and IgG2) as control antibodies. Ab1 was a monoclonal antibody targeting the N-terminal structured region of the protein (residues surrounding Val 342) [13] , while Ab2 was of polyclonal origin targeting unstructured C-terminus [22] (Fig. 1B).

The availability of highly specific antibodies against CIP2A facilitated the IP of endogenous CIP2A without the requirement for overexpression. After preparation for proteomic analysis, the digested samples were analyzed by LC-MS/MS to identify the CIP2A associated proteins. Analysis of the data revealed 680 proteins meeting the criteria of identification of two or more unique peptides with a confidence threshold of 99%. In order to distinguish non-specific interactions and common contaminants, statistical analysis of the LFQ intensity data was made using the Significance Analysis of *INTeractome* (*SAINT*) algorithm [23] . Using a threshold for the calculated SAINT probability scores of greater than or equal to 0.95, and exclusion of proteins represented in the contaminant's repository [24] with a frequency of >60%, the list of candidate interacting proteins was reduced to 331 (**Supplementary Table 1A-C)** with

138 more than 90% overlap in common proteins identified with both antibodies specific to
139 CIP2A **(Fig. 1C; S1D; Supplementary Table 1A-C)**. To exemplify the interactions
140 between CIP2A and its interaction partners, the top fifty (50) common proteins
141 detected with both antibodies based on the detected signal intensity is plotted in the
142 form of heatmap **(Fig. 1D)**.

143 **Distribution of CIP2A interactome between the nucleus and cytoplasm**

144 Analysis of the cellular location of CIP2A in epithelial cells has indicated that it is mainly
145 expressed in the cytoplasm [8] , [22] . Further data indicate some representation in
146 the nuclear fraction of epithelial cancer cells [25] . To evaluate the distribution of
147 CIP2A in Th17 cells, confocal microscopy measurements were conducted in this
148 study. For these measurements, 4,6-diamidino-2-phenylindole (DAPI), and Phalloidin
149 were used to stain the nuclear and cytoplasmic fractions, respectively (**Fig 2A**).
150 Statistical analysis of the confocal microscopy images revealed CIP2A is
151 predominantly located in the cytoplasmic compartment of Th17 cells, in addition to
152 some nuclear expression, (**Fig 2B**). Confirmatory measurements were provided with
153 Western Blot (WB) analysis of the cytoplasmic and nuclear fractionations of 72h
154 polarised Th17 cells. For these experiments, vimentin and tubulin were used as control
155 markers for the nuclear and cytoplasmic fractions, respectively (**Fig 2C; S2A**). Whilst
156 the observed expression of CIP2A was greater in the cytoplasmic region, CIP2A was
157 also detected in the nuclear region of 72h differentiated Th17 cells (**Fig 2C; S2A**).

158 Ingenuity Pathways Analysis (IPA; Qiagen) was used to map cellular locations of the
159 proteins interacting with CIP2A. The analysis revealed that the cytoplasm (42%) and
160 nucleus (43%) constituted the most frequent cellular locations of the associated
161 proteins, whilst the plasma membrane (8%), extracellular space (4%), and undefined

162 (other, 3%) accounted for the remainder (**Fig 2D**). The observed distribution of the
163 proteins detected in the CIP2A interactome is consistent with its association in these
164 compartments in Th17 cells.

165 **Cellular processes regulated by CIP2A interactome**

166 To gain an overview of the biological processes associated with CIP2A, we analyzed
167 the CIP2A interactome data with several Gene Ontology and interaction bioinformatics
168 tools. To collate the known interactions between the proteins, a network was
169 constructed using the STRING database [26] . The resulting network was visualized
170 with Cytoscape [27] revealing "RNA metabolism or splicing" as the process most
171 frequently linked with the associated proteins (**Fig. 3A; Supplementary Table 2 and**
172 **3**). The top 20 proteins associated with RNA metabolic process, RNA splicing via
173 transesterification and RNA splicing via spliceosome are represented in the form of
174 heatmaps (**Fig. S3A-C**). In agreement with these results, a recent phosphoproteome
175 screen also identified RNA splicing as one of the most significantly CIP2A-regulated
176 processes [28] .

177 To provide additional context and an appropriate milieu, functional enrichment analysis
178 was made relative to a combined list of the proteins detected together with those found
179 in a recent cellular proteomics analysis of human Th17 cells [29] rather than relative
180 to a background of the whole genome. For this comparison the bioinformatics tools
181 DAVID [30] , [31] and PANTHER [32] , [33] were used. The enriched Th17 pathways
182 are represented in **Fig. 3B**. Again, mRNA processing and splicing were found to be
183 the most significant biological process linked with CIP2A interactors. Collectively,
184 these results suggest the involvement of CIP2A in multiple processes.

185 IPA analysis was also used to summarize the molecular functions of the CIP2A
186 interacting proteins (**Fig. 3C)**. This revealed enzymes (~24%) as the major functional
187 class of the proteins. In addition, transcription regulators (~7.4%) and transporters
188 (6.1%) are the next major class of proteins. A small fraction of proteins was classified
189 as phosphatases (3.4%), kinases (2.0%), translation regulators and ion channels
190 (1.0% each), cytokines and peptidases (<1% each). For a major fraction of the proteins
191 in CIP2A interactome (54%), however, analysis with the IPA database indicated that
192 no specific function could be assigned (marked as "others" in **Fig 3C**). Overall the IPA
193 analysis indicated that CIP2A interacts with proteins with a variety of different
194 functions. It is possible that via its interaction with these proteins CIP2A regulates a
195 range of processes in different cell types, some of which are as of yet undefined.

196 Thus, the functional and network analysis of the associated proteins revealed how
197 CIP2A and its interacting partners participate in a broad set of essential cellular
198 processes, ranging from RNA metabolic processes and splicing to viral processes.

199 **Validation of the Th17 cell CIP2A protein interactions**

200 Validation experiments were performed to verify the interaction of selected proteins
201 with CIP2A. The choice of targets focused on those with most significant interactions
202 and nodal positions in CIP2A interactome (**Fig. 1D).** The validation experiments were
203 carried out by confocal microscopy, WB, or selected reaction monitoring (SRM)
204 targeted mass spectrometry (MS) analysis. The choice of method depended on the
205 availability of suitable working antibodies or proteotypic peptide signatures, for
206 confocal microscopy and WB or SRM-MS analysis, respectively.

207 SRM-MS analysis provided successful validation of twenty CIP2A interaction partners
208 using immunoprecipitates from three independent biological replicates (**Fig 4A;**
209 **Supplementary Table 4-5**). The results are summarized in **Supplementary Table 5.**
210 We confirmed the known interaction of CIP2A with PP2A regulatory subunit A
211 (PPP2R1A) **(Fig. 4A).** In addition, we identified and validated among the CIP2A
212 interactors, PP2A catalytic subunits PPP2CA and PPP2CB **(Fig. 4A; S4A and**
213 **Supplementary Table 5).**

214 Interestingly, we identified PP1 regulatory (PPP1R18 and PPP1R12A) and catalytic
215 subunits (PPP1CA) as the top CIP2A interacting proteins (**Fig 1D)**. By SRM-MS
216 analysis, further confirmed CIP2A interaction with the catalytic subunits (PPP1CA and
217 PPP1CB) of phosphatase PP1 **(Fig. 4A; S4A and Supplementary Table 5)**. Further,
218 in a recent phospho-proteome analysis of CIP2A-regulated proteins, LMNB1 was
219 found to be dephosphorylated in CIP2A silenced cells [28] and here its interaction
220 was identified and validated in CIP2A interactome by SRM MS analysis **(Fig. 4A).**
221 Previous studies have revealed the interaction of with phosphatase PP2A regulatory
222 A subunit [8] . Accordingly, we observed and validated this interaction with PP2A-A in
223 Th17 cells (**Fig 5A).** Additionally, we validated the interaction with the PP2A catalytic
224 subunit PPP2ACA. Notably, we were also able to validate interaction between CIP2A
225 and PP1 catalytic subunit by co-immunoprecipitation followed by WB **(Fig. 5B).**
226 Interaction of CIP2A with both PPP2ACA, and PPP1CA could be because of high
227 structural similarity of the two proteins [34] . Further, PPP1CA interaction was
228 independently validated by Proximity ligation assay (PLA) **(Fig. 5C)**. The negative
229 control, PLA conducted from same samples without primary antibodies, did not show
230 background signals (**Fig. 5C**).

231 TRIM21 was amongst the most enriched proteins in this interactome, and the
232 interaction was validated by both SRM-MS and PLA confocal microscopy **(Fig 5D).**
233 Interaction with the ubiquitin ligase UBR5 was validated by PLA confocal microscopy,
234 both in Th17 cells and Hela cells (**Fig 5D; Fig S5A**). In addition, WB analysis were
235 made for STAT1, IRF4 and TRIM21, which were consistent with the targeted SRM-
236 MS analysis (**Fig 4A; Fig 5E; Fig S5B-C**). Further, NFKB2 was also confirmed to be
237 a CIP2A interacting protein (**Fig 4A, Fig S4A**) and CIP2A inhibition decreased NF-KB
238 activation (**Fig 5F**). In CIP2A silenced Th17 cells, reduced phosphorylation of P65 was
239 detected by WB analysis (**Fig 5F).**

240 **DISCUSSION**

241 With these analyses of the CIP2A interactome in the Th17 milieu, and in relation to
242 phosphatase biology, we verified the well-known interaction with PP2A-A (PPP2R1A)
243 and PP2A regulatory B subunit **(Supplementary Table 1A-C)**. Previously, Wang et
244 al. (2017) demonstrated direct interaction between CIP2A and PP2A regulatory B
245 subunits B56$\alpha$ and B56$\gamma$ by yeast two-hybrid analysis (Y2H), and Junttila et al. (2007)
246 discovered PP2A-A subunit interaction with CIP2A. In the present report, we detected
247 and validated for the first time the interaction of CIP2A with the PP2A catalytic subunit
248 (PPPCA and PPPCB). All of these interactions were validated with SRM-MS analysis
249 **(Fig. 4A; and Supplementary Table 4-5).**

250 The regulatory (PPP1R18 and PPP1R12A) and catalytic (PPP1CA) subunits of
251 phosphatase PP1 were among the top CIP2A interacting partners. Interaction between
252 CIP2A and PP1 has not been previously shown and further studies are required to
253 demonstrate the importance of PP1 association with CIP2A. Notably, the catalytic
254 subunits of both phosphatases PP2A and PP1 were detected and confirmed in the

255 CIP2A interactome. This interaction could arise due to the structural similarity between
256 catalytic subunits of phosphatases PP2A and PP1. It will be an interesting topic for
257 future studies to determine whether CIP2A engages other catalytic subunits of
258 serine/threonine phosphatases.

259 Previously in studies with T regulatory (Treg) cells, PP2A enhanced catalytic activity
260 was identified as an indispensable element of the suppressive function of Treg cells
261 [1] . Treg cells maintain tolerance and prevent autoimmune diseases by suppressing
262 effector cells and modulating the immune system. It remains to be studied whether the
263 interaction between CIP2A and catalytic subunit of PP2A regulates the suppressive
264 function of Treg cells.

265 In relation to CIP2A and PP1 in autoimmune disease, in rheumatoid arthritis (RA)
266 inflamed synovium, increased expression and activity of phosphatase PP1 and
267 reduced transcriptional activity of FOXP3 through specific dephosphorylation of the
268 Ser418 site has been observed [35] . Intriguingly, CIP2A expression in RA has been
269 associated with the histopathological score of synovitis as well as apoptotic resistance
270 and invasive function of fibroblast-like synoviocytes [36] , [37] . Thus, interaction
271 between CIP2A and PP1 may play a role in regulatory T cell function and inflammation
272 in RA.

273 Several kinases related to T cell receptor (TCR) signaling (i.e. CSK and LCK) [38] ,
274 [39] were identified as CIP2A interactors. The initiation of TCR signalling is regulated
275 by the SRC-related protein tyrosine kinase family, which includes LCK, whereas CSK
276 is a potent inhibitor of TCR signalling [38] . Notably, we have observed reduced T cell

277 activation in CIP2A depleted T cells [21] . It will be interesting to study if the loss of
278 CIP2A binding to LCK or CSK contributes to impaired T cell activation

279 The adaptor protein DOCK8 was amongst the most highly enriched proteins detected
280 in this interactome. Combined immunodeficiency in humans is associated with loss-
281 of-function mutations in the gene encoding DOCK8 [40] . Notably, the phenotype in
282 immunodeficiency due to mutations in the gene encoding the transcription factor
283 STAT3 is very similar to that caused by the loss of DOCK8 [41] . Jabara et al. reported
284 that in B cells DOCK8 and STAT3 are components of the same signalling cascade
285 [42] . In Th17 cells, CIP2A interacts with both DOCK8 and Lyn, and regulates STAT3
286 phosphorylation (Khan MM et al., submitted). It could be revealing to study whether
287 CIP2A regulation of STAT3 phosphorylation is dependent on its interaction with Lyn
288 and DOCK8.

289 Several of the proteins of this interactome have functions related to viral response and
290 interferon signalling, i.e. IFI16, IRF4, MX2, STAT1 and TRIM21. Notably amongst
291 these, the increased activity and DNA binding of IRF4 has previously been found in
292 association with the increased capacity of PP2Ac transgenic T cells to produce IL-17
293 in response to TCR stimulation [2] . CIP2A directly interacts and inhibits PP2A in
294 cancer cells and depletion of CIP2A in T cells results in enhanced IL17 (Khan MM et
295 al., submitted manuscript). On the basis of these associations, the influence of CIP2A
296 interaction on the DNA binding of IRF4 in T cells could be an important focus of future
297 studies.

298 Amongst the CIP2A interacting transcription factors were RUNX1 and STAT1, which
299 were validated by WB and SRM. Future studies could address the relationship

300 between CIP2A and STAT1 in Th cells. RUNX1 is important for the development of
301 Th17 cells as it directly binds the promoter of RORC and mediates transactivation of
302 RORC, a transcription factor important for Th17 cell development [43] . In addition,
303 Runx1 has been reported to bind to the IFNγ locus and induce IFNγ in Th17 cells
304 resulting in development of pathogenic $IL17^+$ $IFN\gamma^+$ Th17 Cells [44] . In view of the
305 latter and regarding the detected interaction between CIP2A and RUNX1, it will be of
306 interest to find out if this interaction plays a role in RUNX1 mediated RORC and IFNγ
307 induction in Th17 cells [43] , [44] .

308 TRIM21, an E3 ubiquitin ligase, was prominent in the CIP2A interactome. TRIM21 has
309 been associated with the pathogenesis of several autoimmune diseases, including
310 systemic lupus erythematosus (SLE) and inflammatory bowel diseases (IBDs).
311 TRIM21 plays a protective role in IBD pathogenesis, possibly through inhibition of Th1
312 and Th17 cell immune responses in the intestinal mucosa [45] – [47] . In view of the
313 detected interaction, it is possible that pathways involving CIP2A are also active in the
314 pathogenesis of autoimmune diseases like SLE and IBD.

315 Beta-spectrin (SPTBN1) was amongst the top most proteins enriched in CIP2A
316 interactome. Beta spectrin is a molecular scaffold protein that is involved in cell shape
317 and the organisation of organelles in the cell [48] . Beta spectrin has been identified
318 as an integral component of beta-amyloid plaques in Alzheimer's disease (AD) and
319 spectrin breakdown products (SBDPs) have been implicated as potential biomarkers
320 for neurodegenerative diseases including AD [49] , [50] . In a recent study of AD,
321 CIP2A was found to be overexpressed and associated with tau hyperphosphorylation,
322 mis-localization and AD-related cellular pathology [14] . In mice, overexpression of

323 CIP2A in the brain induced AD-like cognitive deficits [14] . Future studies may
324 determine whether CIP2A interaction with beta-spectrin modulates protein
325 aggregation in AD pathology.

326 In summary, the results of this study present the first characterisation of CIP2A
327 interactome. In addition to the known interactions with the PP2A protein A and B
328 regulatory subunits, our results detail several novel CIP2A interacting proteins. These
329 include the catalytic subunit of PP2A, as well as regulatory and catalytic subunits of
330 PP1. Gene ontology and pathway analysis of the associated proteins suggest CIP2A
331 to be involved in several cellular functions that it has not been previously linked to.
332 Taken together, we anticipate the new information of proteins depicted in this CIP2A
333 interactome and their associated networks, could be useful in understanding the role
334 of CIP2A in regulating cell signalling and its role in various human disorders.

335 **Methods**

336 **Human CD4+ T cell isolation, activation, and differentiation**

337 Umbilical cord blood was layered on Ficol (GE health Care # 17-1440-03) for isolation
338 of white blood cells. CD4+ T cells were then isolated using the Dynal bead CD4+
339 isolation kit from Invitrogen (Cat #11331D). For activation of T cells, a combination of
340 plate-bound anti-CD3 (Beckman Coulter REF # IM-1304) and soluble anti-CD28
341 (Beckman coulter REF # IM1376) antibodies was used. The Th17 cultured cells were
342 stimulated in presence of IL-6 (20ng/ml, Roche, Cat# 11138600 001); IL-1β (10ng/ml,
343 R&D Systems Cat# 201 LB); TGF-β1 (10ng/ml, R&D Systems Cat# 240); anti-IL-4 (1
344 ug/ml) R&D Systems Cat# MAB204); anti-IFN-γ (1 μg/ml R&D Systems Cat#MAB-
345 285).

346 **Flow cytometry**

347 For Th17 and activated T cells, CCR6 surface staining was performed for Th17 cell
348 culture polarization control. Cells were stained with the antibody (eBioscience) in
349 FACS I buffer (1%FBS in PBS) at +4 °C in darkness for 30min. Cells were then washed
350 two times with FACS I, and finally re-suspended in FACS I Buffer or 1% Formalin
351 before acquisition in BD LSR II/ Caliber. Data analysis was performed using FlowJo
352 (BD) or Flowing Software (Version 2.5.1).

353 **Luminex assay**

354 As a polarization control, IL17 cytokine protein secretion was detected in 72h polarized
355 human Th17 cells and TCR activated control cells. Luminex assay (Milliplex MAP
356 human cytokine, Luminex 200 by Luminex xMAP technology) was used to detect the
357 IL17 cytokine in the supernatant and measured according to the manufacturer's
358 instructions. To avoid cell proliferation bias, the cytokine concentrations were
359 normalized by the number of cells from each respective culture, as counted by flow
360 cytometry.

361 **Immunoprecipitation**

362 CIP2A immunoprecipitation (IP) was carried out with two specific anti-CIP2A
363 antibodies that recognize distinct regions of CIP2A protein and the respective
364 Immunoglobulin G (IgG) were used in control IPs. The Pierce™ MS-Compatible
365 Magnetic IP Kit, (Catalog number: 90409) was used to perform IP. Briefly, cells were
366 first harvested on ice and the culture medium removed. This was followed by washing
367 the cells twice with PBS. Cells were then re-suspended on ice-cold IP-MS Cell Lysis
368 Buffer, as recommended by the manufacturer, and incubated on ice for 10 minutes
369 with periodic mixing. The lysate was centrifuged at ~13,000 × g for 10 minutes to pellet

370 the cell debris. The supernatant was transferred to a new tube for protein
371 concentration determination using a NanoDrop™ spectrophotometer (Thermo
372 Scientific). Cell lysates (500µg) were incubated with the IP antibody (1:50 dilution).
373 The antibody/lysate solution was diluted with the manufacturer's proprietary IP-MS cell
374 lysis buffer and incubated with mixing overnight at +4$^{o}$C to form the immune complex.
375 On the next day the immune complex was incubated with Protein A/G magnetic beads
376 for 1h at room temperature. The beads were then washed and the target antigen eluted
377 with the elution buffer provided and transferred to a new low protein-binding 1.5mL
378 microcentrifuge tube. A vacuum centrifuge was used to dry the eluate prior to
379 preparation for MS or SDS-PAGE and Western blot.

380 **Western Blotting**

381 T cells were first resuspended in Triton-X-100 lysis buffer (TXLB). The composition of
382 TXLB used was 50 mM Tris-HCl (pH 7.5), 150 mM NaCl, 0.5% Triton-X-100, 5%
383 Glycerol, 1% SDS. For cell lysis, T cells in TXLB were then sonicated in ice for 5
384 minutes using a Bioruptor® sonicator. After cell lysis, the lysate was centrifuged at
385 high speed (16,000 g) and the supernatant was transferred to a new tube to remove
386 cell debris. Protein concentration was estimated using a DC Protein assay (Bio-Rad
387 Cat#500-0111). Equal amounts of protein were loaded onto the acrylamide gel (Bio-
388 Rad Mini or Midi PROTEAN® TGX precast gels). For the transfer of proteins to the
389 PVDF membrane, mini or a midi transfer packs from Bio-Rad were used depending
390 on the gel size. Primary/ secondary antibody incubations were performed in 5% non-
391 fat milk or Bovine serum albumin (BSA) for phosphoproteins in TBST buffer
392 (0.1%Tween 20 in Tris-buffered saline). Quantification of the bands detected was
393 performed using Image J software after normalization relative to the loading control

394 intensities. The following antibodies were used for western blotting, CIP2A antibody
395 1(Ab1) (Cell Signaling Technology; cat#14805) CIP2A antibody 2 (Ab2) provided by
396 Prof. Jukka Westermarck [8] , [22] ; PP2A-A/B (sc-15355; Santa Cruz); Trim21
397 antibody (Santa Cruz); Irf4 antibody (Santa Cruz); Beta-actin antibody (Sigma Cat #.
398 A5441). PPP1A/PPP1CA antibody (ab137512; abcam), PP1α Antibody (G-4): (sc-
399 271762; Santa Cruz).

400 **Immunofluorescence**

401 Th17 cells were plated onto acid-washed glass coverslips. The cells were then fixed
402 at room temperature (RT) using 4 % PFA for 10 mins. After fixing, the cells were
403 permeabilized in PBS containing 30% horse serum and 0.1% Triton X-100 for 10 min
404 at RT, washed in PBS and then blocked in PBS-30% horse serum for 1h at RT. The
405 cells were then incubated with the CIP2A primary antibody overnight at 4°C. On the
406 next day, the cells were washed three times using PBS and incubated for 1h at RT
407 with AlexaFluor-conjugated secondary antibodies (Life Technologies). Cells were then
408 mounted with Mowiol® for 30 min at 37°C and Images taken with a Carl Zeiss LSM780
409 laser scanning confocal microscope equipped with 100×1.40 oil plan-Apochromat
410 objective (Zeiss). Corrected total cell fluorescence was calculated from confocal
411 images to quantify the intensities in Th0 and Th17 cells. [51] , [52] .

412 Immunofluorescence staining of UBR5 in Hela cells was performed similarly, the cells
413 were cultured on chambered coverslip (80826, Ibidi). 4% paraformaldehyde was used
414 to fix the cells for 15 minutes under room temperature, and then cells were
415 permeabilized with 0.5% Triton X-100 in PBS on ice for 5 minutes. Next, the cells were
416 blocked with 10% normal goat serum (ab7481, Abcam) diluted in PBS for 30 minutes,
417 and followed by incubating with the primary antibodies anti-UBR5 (ab70311, Abcam)

418 overnight at 4°C. Subsequently, cells were washed with PBS and incubated with the
419 secondary antibody, Alex Fluor 488 goat anti-rabbit IgG (A-11008, Invitrogen) for 1h
420 under room temperature. After secondary antibody incubation, the cells were washed
421 with PBS and nuclei were stained with DAPI (D1306, Invitrogen) in PBS at RT for 10
422 min. Images were acquired with confocal microscope (LSM780, Carl Zeiss).

423 **Proximity ligation assay**

424 The PLA assay was performed according to the manufacturer's protocol (Duolink®
425 PLA, Sigma). Briefly, Th17 or HeLa cells were plated on coverslips. The cells were
426 fixed with 4% paraformaldehyde for 15 minutes at room temperature, and then
427 permeabilized with 0.5% Triton X-100 in PBS on ice for 5 minutes. Next, cells were
428 blocked with blocking solution, and incubated in a pre-heated humidity chamber for 30
429 min at 37°C, followed by incubating with the primary antibodies (in blocking solution)
430 anti-UBR5 (ab70311, Abcam) and anti-CIP2A (sc-80659, Santa Cruz), anti-PPP1CA
431 (ab137512, Abcam), anti-UBR5 (ab70311, Abcam), anti-TRIM21 (SC25351, Santa
432 Cruz), anti-GFP (Mouse, ab1218, Abcam ) and anti-GFP (Rabbit, A11122, Invitrogen)
433 overnight at 4°C. Subsequently, cells were washed with the kit buffer A, and the PLA
434 probe was incubated in a pre-heated humidity chamber for 1h at 37°C, followed by
435 ligase reaction in a pre-heated humidity chamber for 30 minutes at 37°C. Next,
436 amplification polymerase solution for PLA was added, followed by incubating the cells
437 in a pre-heated humidity chamber for 100 minutes at 37°C. After amplification, the
438 coverslips were washed with the kit buffer B, and mounted with DAPI. The PLA signal
439 was detected by using a confocal microscope (LSM780, Carl Zeiss) ) and 3i CSU-W1
440 spinning disk microscope equipped with 100x1.4 O Plan-apochromat objective

441 (Zeiss). PLA signals per cell were calculated by dividing the amount of PLA signal dots
442 in one field of view, determined using Cell Profiler software [53]

443 **Cell transfection with siRNA**

444 Naïve T cells were isolated form the cord blood and four million cells were transfected
445 in 100 µl volume of Opti-MEM™ (Gibco by Life Technologies, cat # 31985-047). Lonza
446 nucleofector was used for siRNA transfections. After nucleofection cells were rested
447 for 48h in RPMI supplemented with 10% serum.

448 The siRNAs (synthesized by Sigma) are shown below:

449 siNT 5´- AAUUCUCCGAACGUGUCACGU -3´ 22;

450 siCIP2A-1 5´-CUGUGGUUGUGUUUGCACUTT-3´1.

451 **LC-MS/MS analysis of the proteomic profiles of the immuno-precipitates**

452 The immuno-precipitates were denatured with 8 M urea and cysteine residues reduced
453 with dithiothreitol then alkylated with iodoacetamide. After digestion with trypsin (37
454 $^{0}$C, 16 hours), the samples were desalted using Empore $C_{18}$ disks (3M, Cat No 2215).
455 Based on using UV absorption measurements with a NanoDrop-1000 UV
456 spectrophotometer (Thermo Scientific), equivalent aliquots of the digested peptides
457 were analyzed in triplicate with an Easy-nLC 1200 coupled to a Q Exactive HF mass
458 spectrometer (Thermo Fisher Scientific). A 20 x 0.1 mm i.d. pre-column was used in
459 conjunction with a 150 mm x 75 $\mu$m i.d. analytical column, both packed with 5 $\mu$m
460 Reprosil $C_{18}$-bonded silica (Dr Maisch GmbH). A separation gradient from 8 to 45% B
461 in 78 min was used at a flow rate of 300 nl/min. The mobile phase compositions were,
462 water with 0.1 % formic acid (A) and 80% acetonitrile 0.1% formic acid (B). The MS/MS
463 data were acquired in positive ion mode with a data dependent acquisition setting for

464 higher-energy C-trap dissociation (HCD) of the 10 most intense ions (m/z 300-2000,
465 charge states > 1+). Further details of the preparation and instrument parameters are
466 available as supplementary information.

467 The LC-MS/MS discovery data are available via the PRIDE [54] partner repository
468 from the ProteomeXchange Consortium with the dataset identifier PXD008983.

469 **LC-MS/MS validation of selected targets**

470 Selected reaction monitoring (SRM) mass spectrometry was used to validate the
471 relative abundance of twenty of the proteins that were found to be associated with the
472 CIP2A immuno- precipitates (**Supplementary Table 4**). Heavy-labeled synthetic
473 peptides (lysine $^{13}C_6$ $^{15}N_2$ and arginine $^{13}C_6$ $^{15}N_4$) analogues for the targets of interest
474 were selected on the basis of their consistency and intensity in the discovery data and
475 obtained from Thermo Scientific. For these validations, three additional cultures were
476 prepared from the cord blood of three donors.

477 Using Skyline software [55] the top five most intense transitions for each peptide were
478 evaluated from the MS/MS spectra of heavy labelled peptides and the relative
479 performance of the native peptides in the spiked validation samples.

480 The validation samples were prepared using the same digestion and desalting
481 protocols used for discovery. These were then spiked with synthetic heavy labelled
482 analogues of the peptide targets and a retention time standard (MSRT1, Sigma) for
483 scheduled selected reaction monitoring. The LC-MS/MS analyses were conducted
484 using Easy-nLC 1000 liquid chromatograph (Thermo Scientific) coupled to a TSQ
485 Vantage Triple Quadrupole Mass Spectrometer (Thermo Scientific). The column
486 configuration was the same as used in the discovery experiments and the peptides

487 were separated using a gradient of 8% to 43% B in 27 min, then to 100% B in 3 min,
488 at a flow rate of 300 nl/min (the mobile phase compositions are as indicate above).
489 The raw SRM data are available through PASSEL [56] with the dataset identifier
490 PASS01186

491 **Data analysis and statistics**

492 The peptide/protein identification was performed in Andromeda search engine [57] ,
493 incorporated in MaxQuant software [58] , with a UniProt human protein sequence
494 database (version June 2016, 20,237 entries). Trypsin digestion with a maximum of
495 two missed cleavages, carbamidomethylation of cysteine as a fixed modification, and
496 methionine oxidation and N-terminal acetylation as variable modifications were used
497 in the search parameters. A false discovery rate (FDR) of 0.01 at the peptide and
498 protein level was applied. MaxQuant's label-free quantification (LFQ) algorithm [59]
499 was used to calculate the relative protein intensity profiles across the samples. The
500 "match between the runs" option was enabled with a time window of 0.7 min.

501 The MaxQuant output was further processed using Perseus [60] . The downstream
502 processing included the removal of contaminants, reverse hits and proteins with less
503 than three valid replicate values in the sample groups (IgG or CIP2A pulldown). To
504 identify the potential interacting proteins, Significance Analysis of *INTeractome*
505 (*SAINT*) analysis was performed [24] using the Resource for Evaluation of Protein
506 Interaction Networks (REPRINT) interface (https://reprint-apms.org/). This algorithm
507 uses the distribution, relative intensity and variation of the prey protein detection to
508 calculate probability scores for the certainty of their interaction with the bait.
509 Additionally, the protein lists were compared against a list of common contaminants
510 identified in a catalogue of immunoprecipitation experiments (CRAPome). The

511 thresholds applied to define the putatively interacting proteins included identification
512 on the basis of two or more unique peptides and a SAINT probability score of ≥ 0.95.
513 Although there was no direct match for our sample type and IP conditions in the
514 contaminants repository database, additional filtering was made to exclude proteins
515 that were more than 60% of the datasets. Skyline was used to design the SRM
516 experiments and process the data generated. The MS Stats (3.8.4) plugin included in
517 the Skyline software was used for the group comparison between cases and controls
518 [61] .

519 **Network analysis**

520 Previously reported protein-protein interactions for the detected CIP2A interacting
521 proteins were downloaded from the STRING functional protein association networks
522 database version 10.5 [26] . Both predicted and known high confidence (interaction
523 score ≥ 0.7) interactions were considered. The resulting network was visualized with
524 Cytoscape version 3.6.0 [27] . Clusters in the network were identified using the Markov
525 clustering algorithm implemented in the Cytoscape plug-in clusterMaker v2 algorithm
526 MCL Cluster [62] with the granularity parameter (inflation value) set to 1.8 as
527 suggested by [63] . The MS intensity differences between CIP2A immuno-precipitates
528 and the IgG controls were calculated as median differences across all replicates in the
529 normalized log2-transformed intensities (color coded as a continuous gradient from
530 white to grey as node inner color in Figure 3A).

531 **Enrichment analysis**

532 The enriched GO biological processes were identified using the Database for
533 Annotation, Visualization and Integrated Discovery (DAVID) version 6.8 [30] , [31]
534 and the Protein Annotation Through Evolutionary Relationship (PANTHER)

535 classification system version 13.0 [32] , [33] . The enrichment analyses were
536 performed using the detected CIP2A interactome as the input and the whole detected
537 Th17 proteome from a Th17 profiling study [29] as the background reference. The
538 GO FAT terms from DAVID, which filter out the broadest, non-specific terms, were
539 considered for calculating the most enriched processes within each identified cluster
540 with more than four members. The GO SLIM terms from PANTHER, which give only
541 the broadest terms and filter the more specific ones, were considered for a summary
542 of the enriched biological processes in the CIP2A interactome. A biological process
543 was considered enriched if it had FDR ≤ 0.05. To summarize the cellular locations and
544 protein classes the protein list was annotated using Ingenuity Pathway Analysis
545 (Qiagen).

546 **ACKNOWLEDGEMENTS**

547 For the cord blood collections, we are thankful to the staff of Turku University Hospital,
548 Maternity Ward, Department of Obstetrics and Gynecology. Marjo Hakkarainen and
549 Sarita Heinonen are acknowledge for excellent technical help. We are thankful to the
550 core facilities at the Turku Bioscience centre namely, the Proteomics facility and Cell
551 Imaging Core (CIC) facility. Biocenter Finland are acknowledged for their support of
552 the latter facilities. The Finnish Centre for Scientific Computing (CSC) is duly acknowledged
553 for their efficient servers and their resources in data analysis. MMK was supported by
554 University of Turku graduate school on Turku Doctoral Programme of Molecular
555 Medicine (TuDMM) as well as a central grant from Finnish Cultural Foundation and
556 T.V. was supported by the Doctoral Programme in Mathematics and Computer
557 Sciences (MATTI) of University of Turku. R.L. was supported by the Academy of
558 Finland, AoF, Centre of Excellence in Molecular Systems Immunology and Physiology

559 Research (2012-2017) grant 250114; by the AoF grants 292335, 294337, 292482,
560 31444, by grants from the JDRF, the Sigrid Jusélius Foundation and the Finnish
561 Cancer Foundation. L.L.E. has received grants from the European Research Council
562 (ERC; grant 677943), the European Union's Horizon 2020 research and innovation
563 program (grant 675395), the AoF (grants 296801 and 304995), the Juvenile Diabetes
564 Research Foundation (JDRF; grant 2-2013-32), the Finnish Funding Agency for
565 Innovation (TEKES; grant 1877/31/2016), and the Sigrid Jusélius Foundation. J.W.
566 was funded by the Sigrid Jusélius Foundation.

567 **ETHICAL APPROVAL**

568 Usage of the blood of unknown donors is approved by the Ethics Committee, Hospital
569 District of Southwest Finland.

570 **AUTHOR CONTRIBUTIONS**

571 M.M.K designed and performed the experiments, analyzed data and prepared figures
572 related to WB, TaqMan-PCR and Flowcytometry, and wrote the manuscript. T.V.
573 analyzed data, prepared figures for network analysis and wrote part of the manuscript.
574 M.H.K. designed and performed the experiments, prepared figures, and wrote part of
575 the manuscript. R.M performed SRM-proteomics, analyzed the proteomics data, and
576 contributed to writing the manuscript. U.U. contributed to the pathway and network
577 analyses and writing of the manuscript. S.D.B performed the proteomics experiments
578 data analysis. E.K performed experiments, and analyzed the data. JW provided
579 scientific expertise, and reagents and edited the manuscript. L.E. designed
580 experiments, supervised the study and edited the manuscript. R.L. designed and
581 supervised the study and wrote the manuscript.

582 **DECLARATION OF INTERESTS**

583 The authors declare no competing interests.

584 **ACCESSION NUMBERS**

585 The mass spectrometry data for the interactome have been deposited with the
586 ProteomeXchange Consortium via the PRIDE [54] partner repository with the dataset
587 identifier PXD008983. The validation data have similarly been submitted to the Peptide
588 Atlas [64] with the identifier PASS01186.

589 **REFERENCES**


590 1. Apostolidis SA, Rodríguez-Rodríguez N, Suárez-Fueyo A, Dioufa N, Ozcan E,
591 Crispín JC, et al. Phosphatase PP2A is requisite for the function of regulatory
592 T cells. Nat Immunol. 2016;17(5):556–64.

593 2. Apostolidis SA, Rauen T, Hedrich CM, Tsokos GC, Crispín JC. Protein
594 phosphatase 2A enables expression of interleukin 17 (IL-17) through
595 chromatin remodeling. J Biol Chem. 2013;288(37):26775–84.

596 3. Eitelhuber AC, Warth S, Schimmack G, Düwel M, Hadian K, Demski K, et al.
597 Dephosphorylation of Carma1 by PP2A negatively regulates T-cell activation.
598 EMBO J. 2011;30(3):594–605.

599 4. Janssens V, Goris J. Protein phosphatase 2A: a highly regulated family of
600 serine/threonine phosphatases implicated in cell growth and signalling.
601 Biochem J. 2001 Feb 1;353(Pt 3):417–39.

602 5. Katsiari CG, Kyttaris VC, Juang Y-T, Tsokos GC. Protein phosphatase 2A is a
603 negative regulator of IL-2 production in patients with systemic lupus
604 erythematosus. J Clin Invest. 2005 Nov;115(11):3193–204.

605 6. Long L, Deng Y, Yao F, Guan D, Feng Y, Jiang H, et al. Recruitment of
606 phosphatase PP2A by RACK1 adaptor protein deactivates transcription factor
607 IRF3 and limits Type I interferon signaling. Immunity. 2014;40(4):515–29.

608 7. Wlodarchak N, Xing Y. PP2A as a master regulator of the cell cycle. Crit Rev
609 Biochem Mol Biol. 2016;51(3):162–84.

610 8. Junttila MR, Puustinen P, Niemelä M, Ahola R, Arnold H, Böttzauw T, et al.
611 CIP2A Inhibits PP2A in Human Malignancies. Cell. 2007;130(1):51–62.

612 9. Laine A, Sihto H, Come C, Rosenfeldt MT, Zwolinska A, Niemelä M, et al.
613 Senescence Sensitivity of Breast Cancer Cells Is Defined by Positive
614 Feedback Loop between CIP2A and E2F1. Cancer Discov. 2013 Feb
615 1;3(2):182–97.

616 10. Niemelä M, Kauko O, Sihto H, Mpindi J-P, Nicorici D, Pernilä P, et al. CIP2A
617 signature reveals the MYC dependency of CIP2A-regulated phenotypes and
618 its clinical association with breast cancer subtypes. Oncogene. 2012 Sep
619 16;31(39):4266–78.

620 11. Khanna A, Pimanda JE, Westermarck J. Cancerous Inhibitor of Protein
621 Phosphatase 2A, an Emerging Human Oncoprotein and a Potential Cancer
622 Therapy Target. Cancer Res. 2013 Nov 15;73(22):6548–53.

623 12. Lucas CM, Milani M, Butterworth M, Carmell N, Scott LJ, Clark RE, et al. High
624 CIP2A levels correlate with an antiapoptotic phenotype that can be overcome
625 by targeting BCL-XL in chronic myeloid leukemia. Leukemia. 2016
626 Jun;30(6):1273–81.

627 13. Wang J, Okkeri J, Pavic K, Wang Z, Kauko O, Halonen T, et al. Oncoprotein
628 CIP2A is stabilized via interaction with tumor suppressor PP2A/B56. EMBO
629 Rep. 2017 Mar 7;18(3):437–50.

630 14. Shentu Y-P, Huo Y, Feng X-L, Gilbert J, Zhang Q, Liuyang Z-Y, et al. CIP2A
631 Causes Tau/APP Phosphorylation, Synaptopathy, and Memory Deficits in

632 Alzheimer's Disease. Cell Rep. 2018 Jul 17;24(3):713–23.

633 15. Guglani L, Khader SA. Th17 cytokines in mucosal immunity and inflammation.
634 Curr Opin HIV AIDS. 2010 Mar;5(2):120–7.

635 16. Kleinewietfeld M, Manzel A, Titze J, Kvakan H, Yosef N, Linker RA, et al.
636 Sodium chloride drives autoimmune disease by the induction of pathogenic
637 TH17 cells. Nature. 2013;496(7446):518–22.

638 17. Kleinewietfeld M, Hafler DA. The plasticity of human Treg and Th17 cells and
639 its role in autoimmunity. Semin Immunol. 2013 Nov 15;25(4):305–12.

640 18. Romani L. Immunity to fungal infections. Nat Rev Immunol. 2011 Apr
641 11;11(4):275–88.

642 19. Bedoya SK, Lam B, Lau K, Larkin J, III. Th17 cells in immunity and
643 autoimmunity. Clin Dev Immunol. 2013;2013:986789.

644 20. Di Cesare A, Di Meglio P, Nestle FO. The IL-23/Th17 Axis in the
645 Immunopathogenesis of Psoriasis. J Invest Dermatol. 2009 Jun
646 1;129(6):1339–50.

647 21. Côme C, Cvrljevic A, Khan MM, Treise I, Adler T, Aguilar-Pimentel JA, et al.
648 CIP2A promotes T-cell activation and immune response to Listeria
649 monocytogenes infection. PLoS One. 2016;11(4):1–18.

650 22. Hoo LS, Zhang JY, Chan EK. Cloning and characterization of a novel 90 kDa
651 'companion' auto-antigen of p62 overexpressed in cancer. Oncogene. 2002
652 Jul;21(32):5006–15.

653 23. Choi H, Larsen B, Lin Z-Y, Breitkreutz A, Mellacheruvu D, Fermin D, et al.
654 SAINT: probabilistic scoring of affinity purification-mass spectrometry data. Nat
655 Methods. 2011 Jan;8(1):70–3.

656 24. Mellacheruvu D, Wright Z, Couzens AL, Lambert J-P, St-Denis NA, Li T, et al.
657 The CRAPome: a contaminant repository for affinity purification–mass
658 spectrometry data. Nat Methods. 2013 Aug 7;10(8):730–6.

659 25. Myant K, Qiao X, Halonen T, Come C, Laine A, Janghorban M, et al. Serine
660 62-Phosphorylated MYC Associates with Nuclear Lamins and Its Regulation
661 by CIP2A Is Essential for Regenerative Proliferation. Cell Rep. 2015 Aug
662 11;12(6):1019–31.

663 26. Szklarczyk D, Morris JH, Cook H, Kuhn M, Wyder S, Simonovic M, et al. The
664 STRING database in 2017: quality-controlled protein-protein association
665 networks, made broadly accessible. Nucleic Acids Res. 2017 Jan
666 4;45(D1):D362–8.

667 27. Shannon P, Markiel A, Ozier O, Baliga NS, Wang JT, Ramage D, et al.
668 Cytoscape: a software environment for integrated models of biomolecular
669 interaction networks. Genome Res. 2003 Nov;13(11):2498–504.

670 28. Kauko O, Imanishi SY, Kulesskiy E, Laajala TD, Yetukuri L, Laine A, et al.
671 Rules for PP2A-controlled phosphosignalling and drug responses. bioRxiv.
672 2018 Feb 26;271841.

673 29. Tripathi SK, Välikangas T, Shetty A, Khan MM, Moulder R, Bhosale SD, et al.
674 Quantitative Proteomics Reveals the Dynamic Protein Landscape during

675 Initiation of Human Th17 Cell Polarization. iScience. 2019 Jan 26;11:334–55.

676 30. Huang DW, Sherman BT, Lempicki RA. Systematic and integrative analysis of
677 large gene lists using DAVID bioinformatics resources. Nat Protoc. 2009 Jan
678 1;4(1):44–57.

679 31. Huang DW, Sherman BT, Lempicki RA. Bioinformatics enrichment tools: paths
680 toward the comprehensive functional analysis of large gene lists. Nucleic Acids
681 Res. 2009 Jan;37(1):1–13.

682 32. Mi H, Huang X, Muruganujan A, Tang H, Mills C, Kang D, et al. PANTHER
683 version 11: expanded annotation data from Gene Ontology and Reactome
684 pathways, and data analysis tool enhancements. Nucleic Acids Res. 2017 Jan
685 4;45(D1):D183–9.

686 33. Mi H, Muruganujan A, Casagrande JT, Thomas PD. Large-scale gene function
687 analysis with the PANTHER classification system. Nat Protoc. 2013 Jul
688 18;8(8):1551–66.

689 34. Shi Y. Serine/Threonine Phosphatases: Mechanism through Structure. Cell.
690 2009 Oct 30;139(3):468–84.

691 35. Nie H, Zheng Y, Li R, Guo TB, He D, Fang L, et al. Phosphorylation of FOXP3
692 controls regulatory T cell function and is inhibited by TNF-α in rheumatoid
693 arthritis. Nat Med. 2013 Mar 10;19(3):322–8.

694 36. Lee J, Park E-J, Hwang JW, Oh J-M, Kim H, Bae E-K, et al. CIP2A expression
695 is associated with synovial hyperplasia and invasive function of fibroblast-like
696 synoviocytes in rheumatoid arthritis. Rheumatol Int. 2012 Jul 9;32(7):2023–30.

697 37. Lee J, Jeong H, Park E-J, Hwang JW, Huang B, Bae E-K, et al. CIP2A
698 facilitates apoptotic resistance of fibroblast-like synoviocytes in rheumatoid
699 arthritis independent of c-Myc expression. Rheumatol Int. 2013 Sep
700 2;33(9):2241–8.

701 38. Chow LML, Fournel M, Davidson D, Veillette A. Negative regulation of T-cell
702 receptor signalling by tyrosine protein kinase p50 csk. Nature. 1993 Sep
703 9;365(6442):156–60.

704 39. Veillette A, Latour S, Davidson D. N EGATIVE R EGULATION OF I
705 MMUNORECEPTOR S IGNALING. Annu Rev Immunol. 2002 Apr;20(1):669–
706 707.

707 40. Zhang Q, Davis JJC, Lamborn IT, Freeman AF, Jing H, Favreau AJ, et al.
708 Combined Immunodeficiency Associated with *DOCK8* Mutations. N Engl J
709 Med. 2009 Nov 19;361(21):2046–55.

710 41. Su HC. Dedicator of cytokinesis 8 (DOCK8) deficiency. Curr Opin Allergy Clin
711 Immunol. 2010 Dec;10(6):515–20.

712 42. Jabara HH, McDonald DR, Janssen E, Massaad MJ, Ramesh N, Borzutzky A,
713 et al. DOCK8 functions as an adaptor that links TLR-MyD88 signaling to B cell
714 activation. Nat Immunol. 2012 May 13;13(6):612–20.

715 43. Lazarevic V, Chen X, Shim J-H, Hwang E-S, Jang E, Bolm AN, et al. T-bet
716 represses TH17 differentiation by preventing Runx1-mediated activation of the
717 gene encoding RORγt. Nat Publ Gr. 2010;12.

718 44. Wang Y, Godec J, Ben-Aissa K, Cui K, Zhao K, Pucsek AB, et al. The

719 transcription factors T-bet and runx are required for the ontogeny of
720 pathogenic interferon-γ-producing T helper 17 cells. Immunity.
721 2014;40(3):355–66.

722 45. Espinosa A, Dardalhon V, Brauner S, Ambrosi A, Higgs R, Quintana FJ, et al.
723 Loss of the lupus autoantigen Ro52/Trim21 induces tissue inflammation and
724 systemic autoimmunity by disregulating the IL-23–Th17 pathway. J Exp Med.
725 2009 Aug 3;206(8):1661–71.

726 46. Yoshimi R, Ishigatsubo Y, Ozato K. Autoantigen TRIM21/Ro52 as a Possible
727 Target for Treatment of Systemic Lupus Erythematosus. Int J Rheumatol.
728 2012;2012:718237.

729 47. Zhou G, Wu W, Yu L, Yu T, Yang W, Wang P, et al. Tripartite motif-containing
730 (TRIM) 21 negatively regulates intestinal mucosal inflammation through
731 inhibiting TH1/TH17 cell differentiation in patients with inflammatory bowel
732 diseases. J Allergy Clin Immunol. 2017 Nov 4;

733 48. Machnicka B, Grochowalska R, Bogusławska DM, Sikorski AF, Lecomte MC.
734 Spectrin-based skeleton as an actor in cell signaling. Cell Mol Life Sci. 2012
735 Jan;69(2):191–201.

736 49. Sihag RK, Cataldo AM. Brain beta-spectrin is a component of senile plaques in
737 Alzheimer's disease. Brain Res. 1996 Dec 16;743(1–2):249–57.

738 50. Yan X-X, Jeromin A, Jeromin A. Spectrin Breakdown Products (SBDPs) as
739 Potential Biomarkers for Neurodegenerative Diseases. Curr Transl Geriatr Exp
740 Gerontol Rep. 2012 Jun;1(2):85–93.

741 51. Burgess A, Vigneron S, Brioudes E, Labbé J-C, Lorca T, Castro A. Loss of
742 human Greatwall results in G2 arrest and multiple mitotic defects due to
743 deregulation of the cyclin B-Cdc2/PP2A balance. Proc Natl Acad Sci U S A.
744 2010 Jul 13;107(28):12564–9.

745 52. McCloy RA, Rogers S, Caldon CE, Lorca T, Castro A, Burgess A. Partial
746 inhibition of Cdk1 in $G_2$ phase overrides the SAC and decouples mitotic
747 events. Cell Cycle. 2014 May 6;13(9):1400–12.

748 53. Carpenter AE, Jones TR, Lamprecht MR, Clarke C, Kang I, Friman O, et al.
749 CellProfiler: image analysis software for identifying and quantifying cell
750 phenotypes. Genome Biol. 2006;7(10):R100.

751 54. Vizcaíno JA, Csordas A, del-Toro N, Dianes JA, Griss J, Lavidas I, et al. 2016
752 update of the PRIDE database and its related tools. Nucleic Acids Res. 2016
753 Jan 4;44(D1):D447–56.

754 55. MacLean B, Tomazela DM, Shulman N, Chambers M, Finney GL, Frewen B,
755 et al. Skyline: an open source document editor for creating and analyzing
756 targeted proteomics experiments. Bioinformatics. 2010 Apr 1;26(7):966–8.

757 56. Farrah T, Deutsch EW, Kreisberg R, Sun Z, Campbell DS, Mendoza L, et al.
758 PASSEL: the PeptideAtlas SRMexperiment library. Proteomics. 2012
759 Apr;12(8):1170–5.

760 57. Cox J, Neuhauser N, Michalski A, Scheltema RA, Olsen J V., Mann M.
761 Andromeda: A Peptide Search Engine Integrated into the MaxQuant
762 Environment. J Proteome Res. 2011 Apr 1;10(4):1794–805.

763 58. Cox J, Mann M. MaxQuant enables high peptide identification rates,
764 individualized p.p.b.-range mass accuracies and proteome-wide protein
765 quantification. Nat Biotechnol. 2008 Dec 30;26(12):1367–72.

766 59. Cox J, Hein MY, Luber CA, Paron I, Nagaraj N, Mann M. Accurate Proteome-
767 wide Label-free Quantification by Delayed Normalization and Maximal Peptide
768 Ratio Extraction, Termed MaxLFQ. Mol Cell Proteomics. 2014
769 Sep;13(9):2513–26.

770 60. Tyanova S, Temu T, Sinitcyn P, Carlson A, Hein MY, Geiger T, et al. The
771 Perseus computational platform for comprehensive analysis of (prote)omics
772 data. Nat Methods. 2016 Sep 27;13(9):731–40.

773 61. Choi M, Chang C-Y, Clough T, Broudy D, Killeen T, MacLean B, et al.
774 MSstats: an R package for statistical analysis of quantitative mass
775 spectrometry-based proteomic experiments. Bioinformatics. 2014 Sep
776 1;30(17):2524–6.

777 62. Morris JH, Apeltsin L, Newman AM, Baumbach J, Wittkop T, Su G, et al.
778 clusterMaker: a multi-algorithm clustering plugin for Cytoscape. BMC
779 Bioinformatics. 2011 Nov 9;12(1):436.

780 63. Brohée S, van Helden J. Evaluation of clustering algorithms for protein-protein
781 interaction networks. BMC Bioinformatics. 2006 Nov 6;7(1):488.

782 64. Desiere F, Deutsch EW, King NL, Nesvizhskii AI, Mallick P, Eng J, et al. The
783 PeptideAtlas project. Nucleic Acids Res. 2006 Jan 1;34(Database
784 issue):D655-8.

785 **FIGURE LEGENDS**

786 **Figure 1. CIP2A interactome top protein interaction in Th17 cells.**

787 **(A)** Western Blot (WB) analysis of CIP2A immunoprecipitated (IP) with two antibodies
788 (Ab1 and Ab2) specific to different regions of CIP2A in 72h polarised Th17 cells. For
789 each CIP2A targeting antibody, an IgG control antibody (IgG1 and IgG2) was used.
790 The figure is a representative WB of two experiments. Input, IgG control IP and CIP2A
791 IP reactions are shown.

792 **(B)** Schematic diagram of the human CIP2A protein structure. Regions specific to the
793 antibodies used in the pulldown are shown. Ab1: against residues surrounding valine
794 343 (monoclonal), Ab2: 618-905 peptide (polyclonal). Protein domain borders are
795 based on previous publication (Wang et al., 2017) in which the Armadillo repeat, and
796 the dimerization interface are shown in the CIP2A structured domain studied by Wang
797 et al., 2017.

798 **(C)** A Venn diagram showing the number of common and unique CIP2A interacting
799 proteins identified with two distinct antibodies targeting CIP2A based on the mass
800 spectrometry (ms) analysis. For details, please see the method section.

801 **(D)** Heatmap representation of the top fifty CIP2A interactors identified with both
802 antibodies. R1 and R2 represent data from two biological replicates. Normalized
803 spectral intensities are plotted as a heatmap to display protein abundance in
804 respective IP reactions.

805 **Figure 2. Cellular distribution of CIP2A and the proportions of CIP2A**
806 **interactome in Th17 cells.**

807 **(A)** Immunostaining for the study of CIP2A localisation in 72h polarised Th17 cells. A
808 representative image of three replicates are shown. Cells were stained for
809 endogenous CIP2A (green). Phalloidin (red) and DAPI (blue) were used to stain
810 cytoplasmic and nuclear regions, respectively. Scale bar is 7μm.

811 **(B)** Statistical analyses of CIP2A expression for cellular localization studies from three
812 replicates using GraphPad Prism version 8.0d for Mac OS X (GraphPad Software).
813 Statistical analysis was made by a two-tailed paired Student's T-test, where p-value **
814 represent <0.01. The error bars represent standard error of the mean.

815 **(C)** Representative WB analysis of CIP2A localisation in the cytoplasmic and nuclear
816 fractions of 72h polarised Th17 cells. Vimentin and Tubulin were used as controls for
817 the nuclear and cytoplasmic fractions, respectively. WCL: Whole Cell lysate, NF:
818 Nuclear Fraction, and CF: Cytoplasmic Fraction.

819 **(D)** Enriched cellular locations of the proteins in the CIP2A interactome presented in
820 the form of pie chart. The enrichment analysis was performed using the Ingenuity
821 pathway analysis (IPA; Qiagen).

822 **Figure 3. The CIP2A protein interaction network.**

823 **(A)** The interaction network among the CIP2A interacting proteins. Protein-protein
824 interactions for the network were downloaded from the STRING database and
825 visualized using the Cytoscape software. Nodes in the network were clustered using
826 the Markov clustering algorithm. The identified clusters with more than two members
827 are indicated by distinct colours. A representative GO biological process term is shown
828 for each cluster with four or more members. The GO enrichment analysis was

829 performed using DAVID against a Th17 proteome reference background (Tripathi et
830 al., 2019). The median MS intensity differences between the CIP2A immuno-
831 precipitates and the IgG controls are shown as node inner colour from white to grey
832 according to increasingly stronger expression in the CIP2A immuno-precipitates
833 compared to the IgG controls.

834 **(B)** Enriched Biological processes associated with the proteins in the CIP2A
835 interactome in human Th17 cells. The enrichment analyses was performed using
836 PANTHER with the enrichment calculated from a background of proteins detected in
837 Th17 proteomic reference background (Tripathi et al., 2019). The scale is –log FDR.

838 **(C)** Functional classification of the CIP2A interactome in Th17 cells. The proportions
839 of different enriched functional classes in the CIP2A interacting proteins. The
840 enrichment analysis was performed using IPA (Qiagen).

841 **Figure 4. CIP2A interactome validation by SRM mass spectrometry.**

842 Selected reaction monitoring targeted mass spectrometry (SRM-MS) validation of the
843 CIP2A interactome. CIP2A IP was performed using antibody Ab2 in 72h polarised
844 Th17 cells and twenty proteins were validated by targeted SRM-MS. Averaged results
845 from three replicates are presented in the form of a box plot. Statistical analysis was
846 made by a two-tailed paired Student's T-test, where * p-value <0.05; and *** p-value
847 <0.001. The error bars represent 95% confidence interval.

848 **Figure 5. Validation of CIP2A known interaction by Western Blot and Confocal**
849 **microscopy.**

850 **(A)** CIP2A IP performed in Th17 cells and WB detection to validates CIP2A known

851 interaction with phosphatase PP2A-A. Total lysate (Input) and control IP (IgG) and
852 CIP2A IP using Ab2 are shown on the blot. A conformational specific secondary
853 antibody was used to probe proteins without interference from the denatured IgG
854 heavy (50 kDa) and light chains (25 kDa).

855 **(B)** WB validation of the CIP2A-PPP1CA interaction. CIP2A immunoprecipitated with
856 two different antibodies (Ab1 and Ab2) in Th17 cells (72h) and detected as in A.

857 **(C-D)** Proximity ligation assay (PLA) assay validation of the CIP2A-PPP1CA
858 interaction (C) or selected proteins (TRIM21 and UBR5) interaction with CIP2A in Th17
859 cells (D). The GFP antibody was used as a negative control in PLA. DAPI was used
860 to stain the nuclei. Bar is 7μm. Representation of the interaction between CIP2A-
861 PPP1CA (C) or TRIM21 and UBR5 with CIP2A (D) by PLA as a univariate dot plot.
862 Average number of PLA signals (spots) per cell (n=10 images from a representative
863 of three experiments) was plotted. Statistics by paired two tailed T-test, where *
864 represents $P < 0.05$. and ** $< 0.01$. Scale bar is 7μm

865 (**E**) WB validation represent interactions between TRIM21, IRF4, STAT1 and PP2A
866 with CIP2A in Th17 cells at 72h and CIP2A. IP was performed using Ab2 and
867 conformational specific secondary antibody was used as in Fig. 2C.

868 **(F)** CIP2A inhibition leads to decreased TNFα-elicited Nf-κB activation. Total and
869 phospho-p65 (pp65) Nf-κB subunit expression in CIP2A silenced and control Th17
870 cells. CIP2A is silenced in three different individual donor cell pools, and CIP2A, pp65,
871 p65 and Actin are shown on the blot.

872

873 **SUPPLEMENTARY FIGURE LEGENDS**

874 **Figure S1 (Related to Figure 1). The polarization of the Th17 cultures used in the**
875 **study and a schematic representation of the interactome study.**

876 **(A)** The proportion of CCR6+ cells from the flow-cytometry analysis of CCR6 surface
877 expression at 72h in TCR activated control Th0 cells and polarized Th17 cells. The
878 IL17A mRNA expression (**B**), and IL17A protein secretion (**C**) from the cultures at 72h
879 post initiation of Th17 polarization. The data (**A**-**C**) is from six independent cultures
880 and each culture consisted of cells from more than four individual donors. Error bars
881 represent SEM estimates across biological replicates and P-values calculated using
882 the paired two-tailed student's t-test. (n = 6; P <0.01(**) and P <0.001(***) for Th0 vs
883 Th17). (**D**) A schematic layout representation of the interactome study.

884 **Figure S2 (Related to Figure 2).**

885 WB analysis of two replicates for the cytoplasmic and nuclear fractions for CIP2A sub-
886 cellular localisation in 72h polarised Th17 cells. WB probes with antibodies as controls
887 for nuclear and cytoplasmic fractions detecting Vimentin and Tubulin proteins,
888 respectively. WCL, NF and CF represent Whole Cell lysate, Nuclear Fraction, and
889 Cytoplasmic Fraction respectively.

890 **Figure S3 (Related to Figure 3). The normalized expression of the top CIP2A**
891 **interacting proteins in selected highly enriched GO biological processes in the**
892 **detected CIP2A interactome.**

893 The 20 strongest CIP2A interacting proteins in the **A**) RNA metabolic process (**B**) RNA
894 splicing via transesterification and (**C**) RNA splicing via spliceosome enriched GO

895 biological processes. The expression values are normalized $log_2$ transformed protein
896 intensities from the MS analysis of the CIP2A immuno-precipitates (IP) and the IgG
897 controls. The expression values for both antibodies (Ab1 and Ab2) specific to different
898 regions for two individual replicates are shown. The proteins in each heatmap are in
899 descending order based on the median expression differences between the CIP2A-
900 IPs and the IgG controls.

901 **Figure S4 (Related to Figure 4).**

902 The averaged logarithmic fold changes and logarithmic significance values (log FDR)
903 for the targeted mass spectrometry (SRM-MS) validations analysis of the twenty
904 selected (shown in Figure 4A) proteins from the CIP2A interactome.

905 **Figure S5 (Related to Figure 5).**

906 **(A)** UBR5 immunostaining in Hela cells and PLA validation for interaction between
907 CIP2A and UBR5 by confocal microscopy. For PLA, the antibodies were used as
908 negative controls. DAPI was used to stain nuclei. Bar = 10µm

909 **(B-C)** WB validations of selected proteins in CIP2A interactome (Two replicates). (**B**)
910 First replicate showing two separate blots, TRIM21 and IRF4 (first blot) and STAT1
911 and PP2A (second blot). (**C**) WB validations of the second replicate for the same
912 proteins. CIP2A pull-down in 72h polarised Th17 cells and CIP2A IP, IgG control IP
913 and Input reactions are shown on the blot. CIP2A IP was performed using Ab2 and
914 conformational specific secondary antibody was used to probe proteins without
915 interference from denatured IgG heavy (50 kDa) and light chains (25 kDa).

916

917 **SUPPLEMENTRY TABLE LEGENDS**

918 **Supplementary Table S1 (A-C). CIP2A interactome in Th17 cells. (**Related to Fig.
919 1). Table list proteins associated with the CIP2A interactome (**Supplementary Table**
920 **S1A)**. The table also list Ingenuity Pathway Analysis (IPA) cellular location and
921 functional class assigned IPA annotation for the proteins detected in the CIP2A
922 interactome (**Supplementary Table S1B)**. The CIP2A interactome associated
923 proteins information are listed together with the data from the MaxQuant results
924 (unique peptides, sequence coverage, intensity and Andromeda score),
925 representation in the CRAPome, and SAINT analysis showing Saint Probability (SP)
926 (**Supplementary Table S1C)**. The data is filtered to only include proteins with a SP
927 values of > 0.95 and less than 60% representation in the CRAPOME.

928 **Supplementary Table S2.** (Related to Fig. 3). **The 20 most enriched GO FAT**
929 **biological processes (BP) in each cluster of the CIP2A interactome network in**
930 **Figure 3A.** The GO enrichment was performed using DAVID (Huang et al., 2009)
931 against a Th17 proteome reference background (Tripathi et al., 2019). The GO FAT
932 BP terms, which filter out the broadest higher level GO terms, were considered for
933 more specific enrichment information. For each cluster with four or more members, 20
934 of the most frequently occurring GO FAT terms among the cluster members are listed.
935 For each term, the number of cluster members (proteins or nodes) with the term, the
936 proportion of cluster members with the term, cluster number and annotation for the
937 cluster in Figure 3A, is shown**.**

938 **Supplementary Table S3. (**Related to Fig. 3). **The enriched GO biological**
939 **processes in the detected CIP2A interactome.** The enrichment analysis was

940 performed using PANTHER (Mi et al., 2013, 2017) against a Th17 proteome reference
941 background (Tripathi et al., 2019). The broad GO SLIM terms, which include only the
942 higher level GO terms, were considered for a functional summary of the interactome.
943 Fold enrichment, significance value (p-value) and false discovery rate is presented for
944 each term.

945 **Supplementary Table S4. SRM Targets for the CIP2A interactome validations.**
946 **(**Associated with Fig. 4 ). The table lists the peptides, associated transitions, collision
947 energies and retention time windows used for the SRM validations of the CIP2A vs.
948 control IgG pull downs.

949 **Supplementary Table S5. SRM MS CIP2A interactome validations. (**Associated
950 with Fig. 4 ). The table lists the $log_2$ transformed relative abundance data from the
951 SRM analysis of the CIP2A IP vs. control IgG pull downs from three biological
952 replicates for proteins validated for the CIP2A interactome.

Figure 1

A

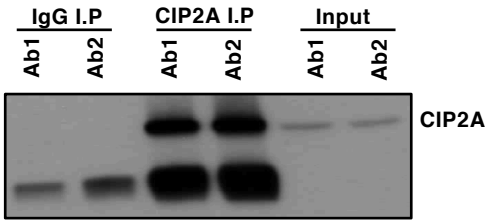


B

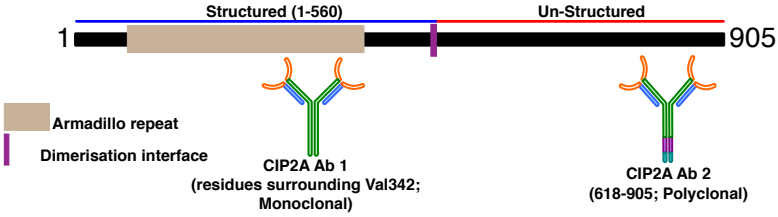


C

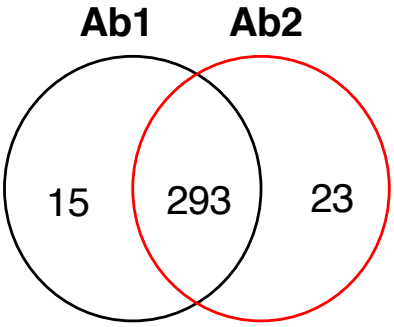


D

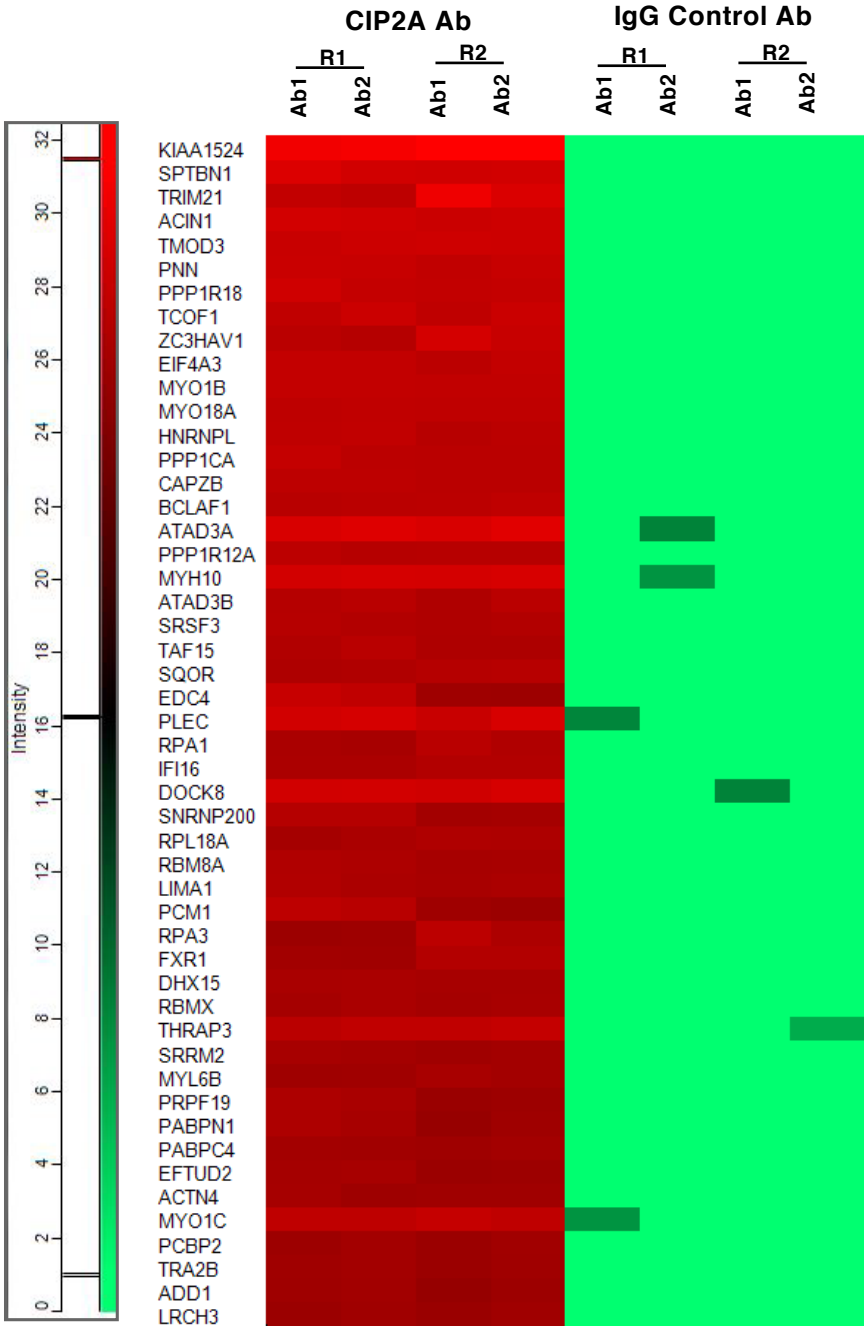

Figure 2

A

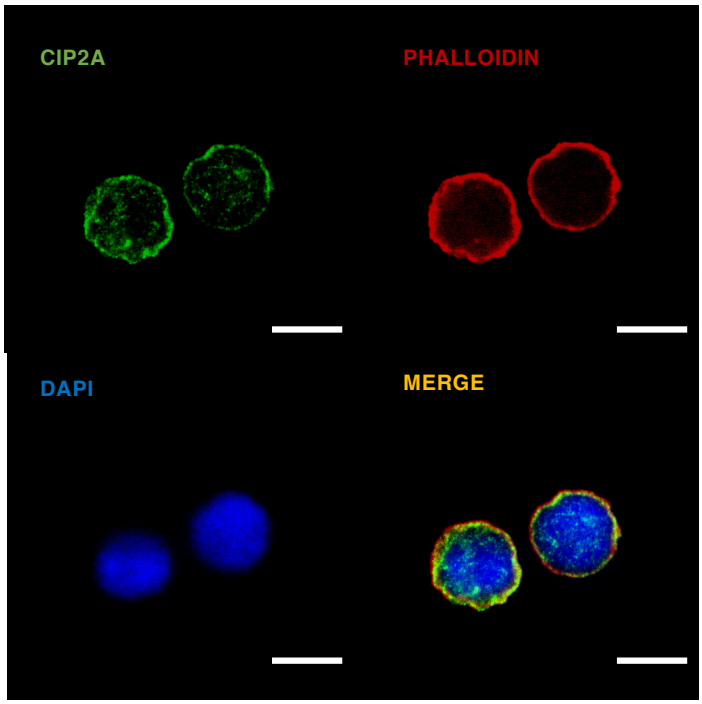


B

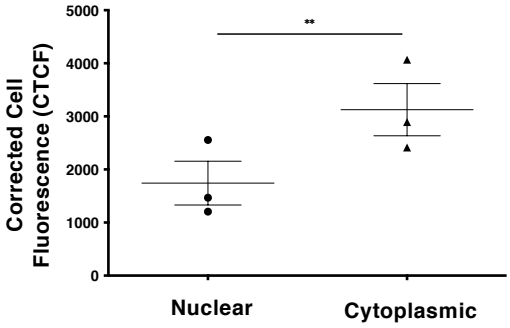


C

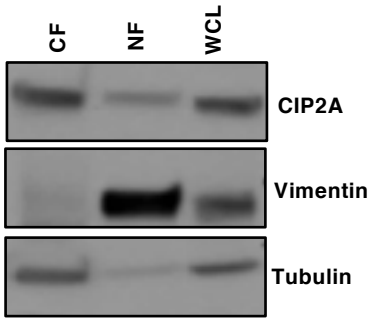


D

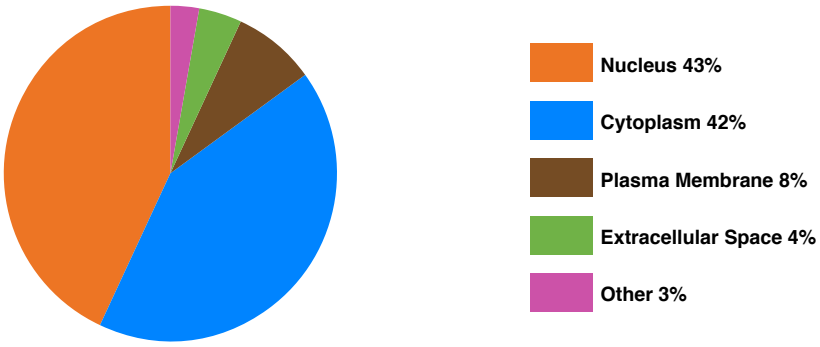

**Figure 3**

A

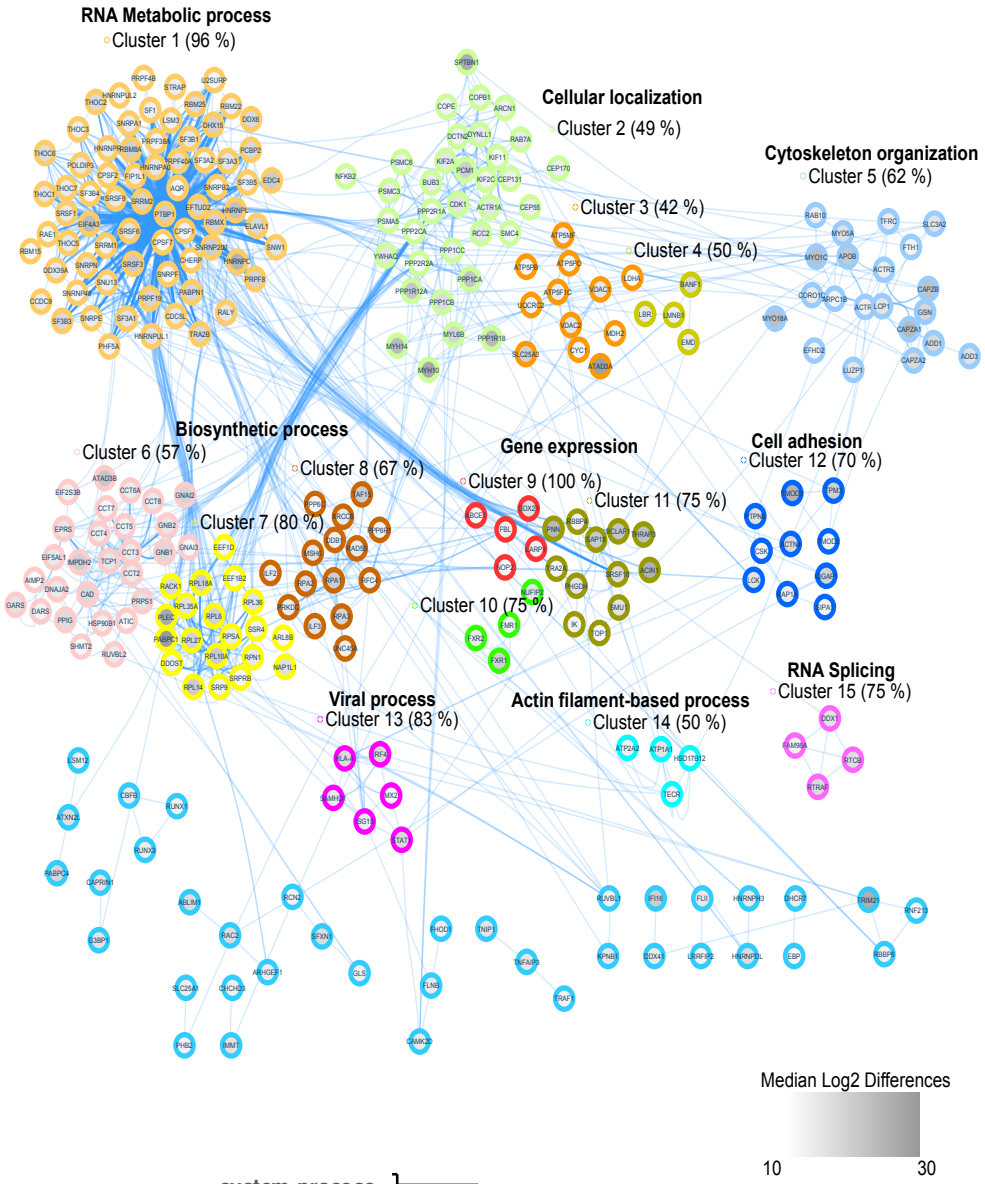
RNA Metabolic process
Cluster 1 (96 %)
Cellular localization
Cluster 2 (49 %)
Cluster 3 (42 %)
Cluster 4 (50 %)
Cytoskeleton organization
Cluster 5 (62 %)
Biosynthetic process
Cluster 6 (57 %)
Cluster 7 (80 %)
Cluster 8 (67 %)
Gene expression
Cluster 9 (100 %)
Cluster 10 (75 %)
Cluster 11 (75 %)
Cell adhesion
Cluster 12 (70 %)
Viral process
Cluster 13 (83 %)
Actin filament-based process
Cluster 14 (50 %)
RNA Splicing
Cluster 15 (75 %)
Median Log2 Differences
10
30

B

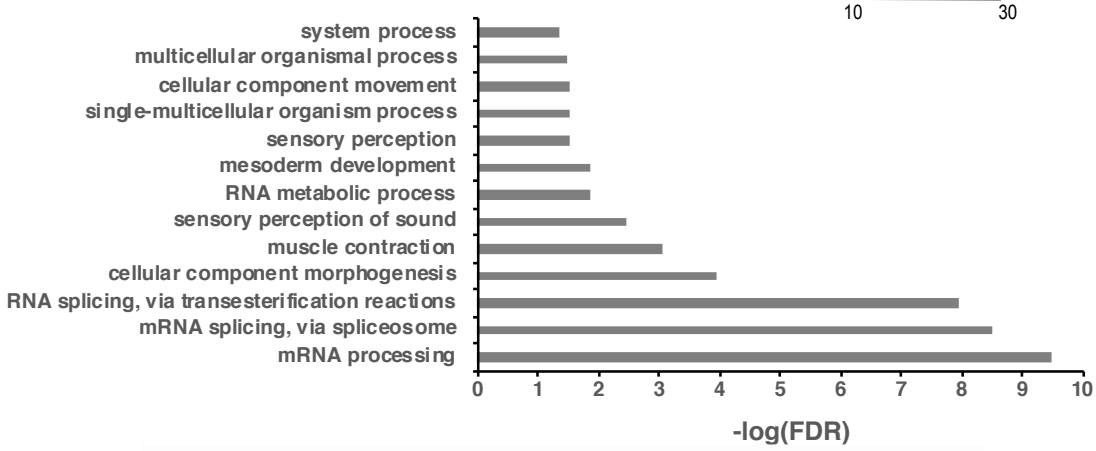
system process
multicellular organismal process
cellular component movement
single-multicellular organism process
sensory perception
mesoderm development
RNA metabolic process
sensory perception of sound
muscle contraction
cellular component morphogenesis
RNA splicing, via transesterification reactions
mRNA splicing, via spliceosome
mRNA processing
0
1
2
3
4
5
6
7
8
9
10
-log(FDR)

C

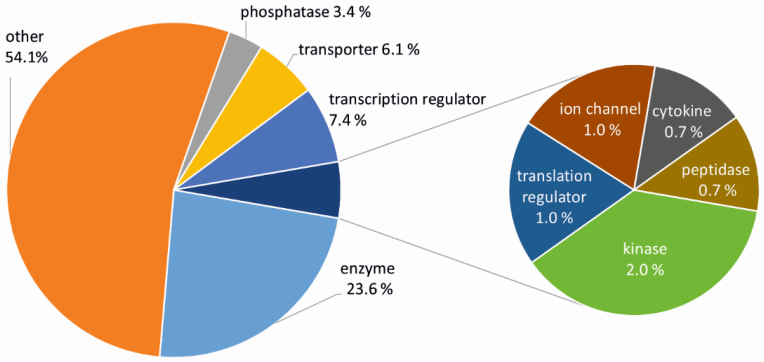
other
54.1%
phosphatase 3.4 %
transporter 6.1 %
transcription regulator
7.4 %
enzyme
23.6 %
ion channel
1.0 %
cytokine
0.7 %
peptidase
0.7 %
translation
regulator
1.0 %
kinase
2.0 %

**Figure 4**

**A**

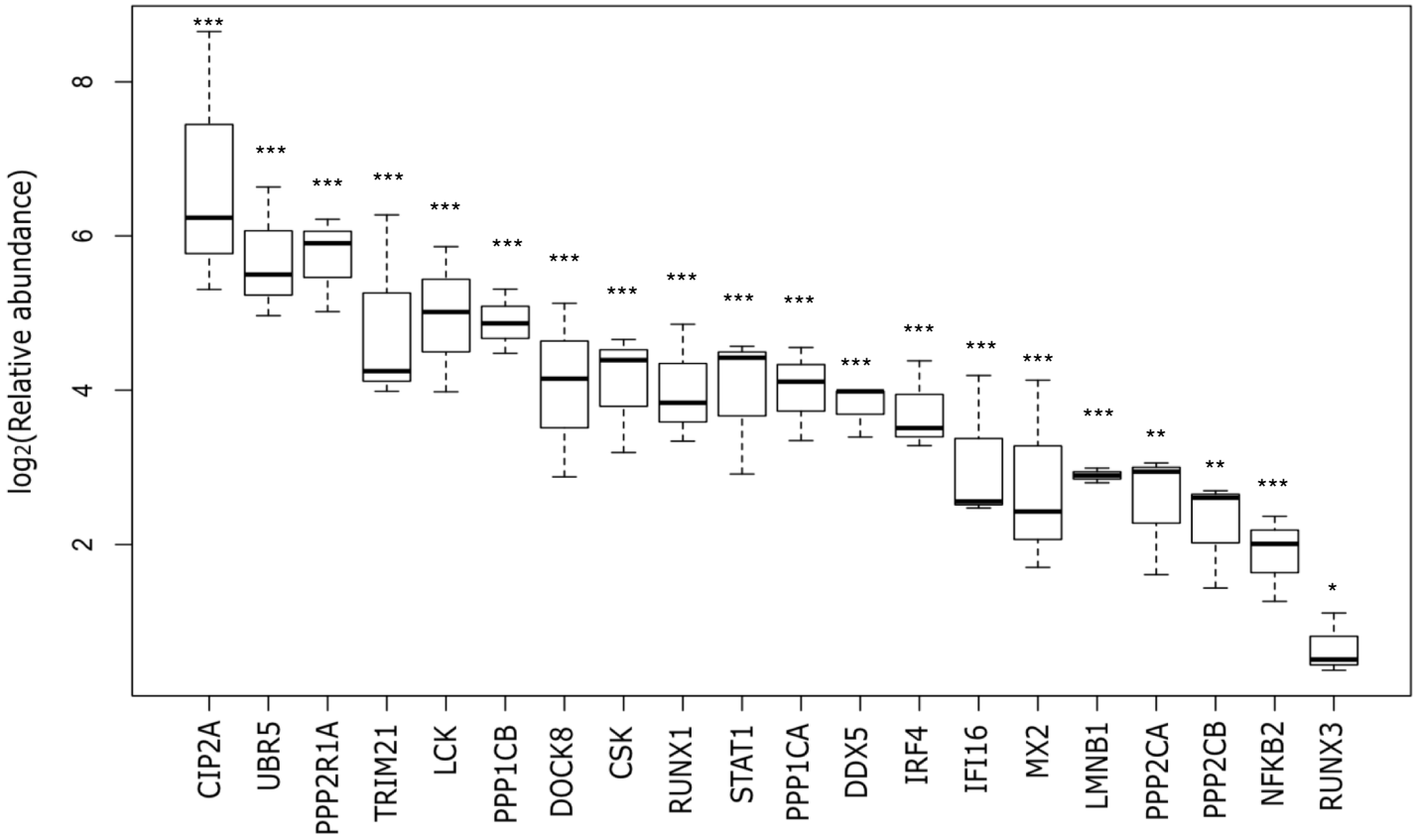
log2(Relative abundance)
2
4
6
8
CIP2A
UBR5
PPP2R1A
TRIM21
LCK
PPP1CB
DOCK8
CSK
RUNX1
STAT1
PPP1CA
DDX5
IRF4
IFI16
MX2
LMNB1
PPP2CA
PPP2CB
NFKB2
RUNX3
***
**
*

Figure 5

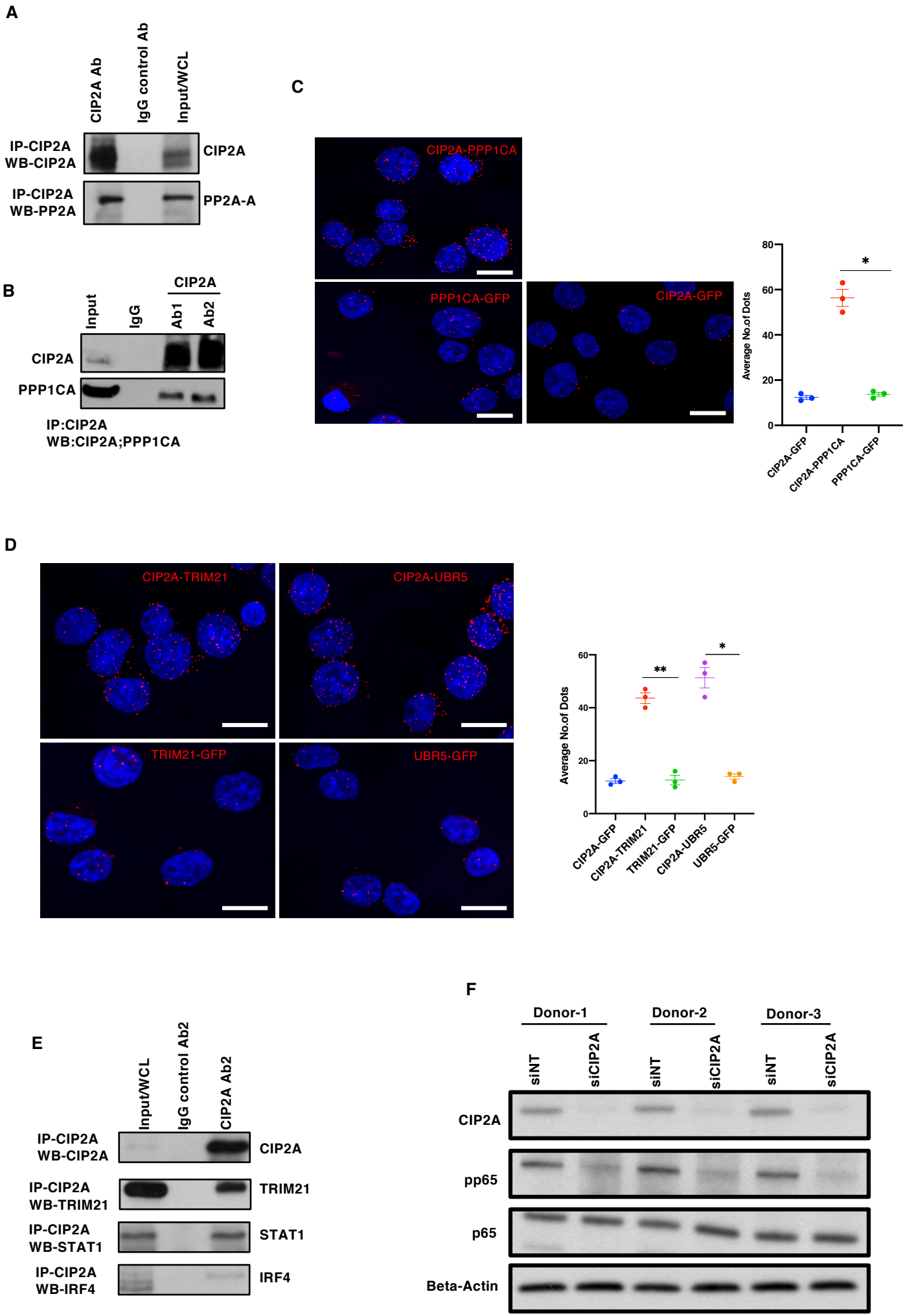
A
CIP2A Ab
IgG control Ab
Input/WCL
IP-CIP2A
WB-CIP2A
CIP2A
IP-CIP2A
WB-PP2A
PP2A-A
B
CIP2A
Input
IgG
Ab1
Ab2
CIP2A
PPP1CA
IP:CIP2A
WB:CIP2A;PPP1CA
C
CIP2A-PPP1CA
PPP1CA-GFP
CIP2A-GFP
Average No.of Dots
80
60
40
20
0
*
CIP2A-GFP
CIP2A-PPP1CA
PPP1CA-GFP
D
CIP2A-TRIM21
CIP2A-UBR5
TRIM21-GFP
UBR5-GFP
Average No.of Dots
60
40
20
0
**
*
CIP2A-GFP
CIP2A-TRIM21
TRIM21-GFP
CIP2A-UBR5
UBR5-GFP
E
Input/WCL
IgG control Ab2
CIP2A Ab2
IP-CIP2A
WB-CIP2A
CIP2A
IP-CIP2A
WB-TRIM21
TRIM21
IP-CIP2A
WB-STAT1
STAT1
IP-CIP2A
WB-IRF4
IRF4
F
Donor-1
Donor-2
Donor-3
siNT
siCIP2A
siNT
siCIP2A
siNT
siCIP2A
CIP2A
pp65
p65
Beta-Actin

**Supplementary Figure S1** (Related to Figure 1)

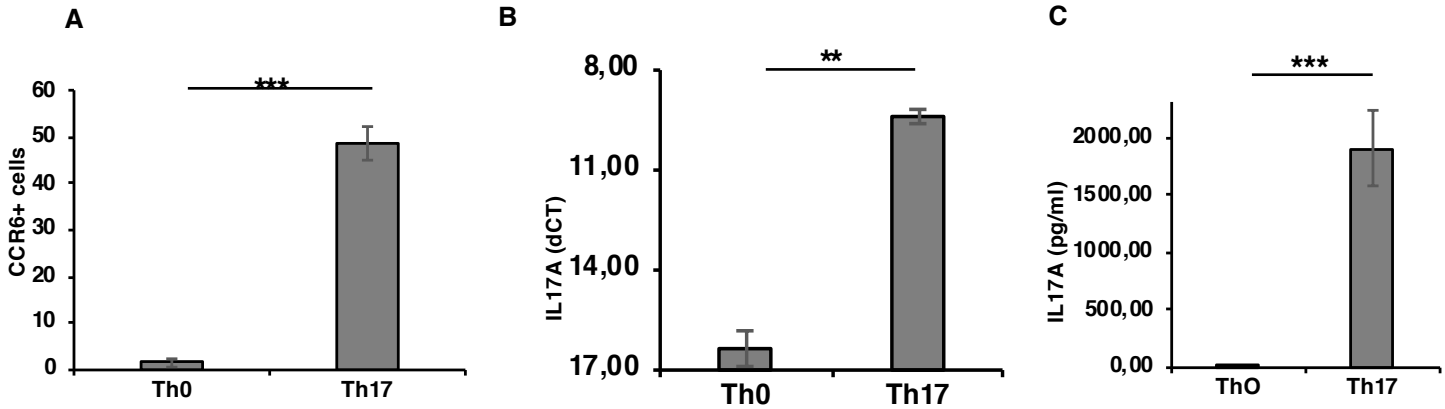


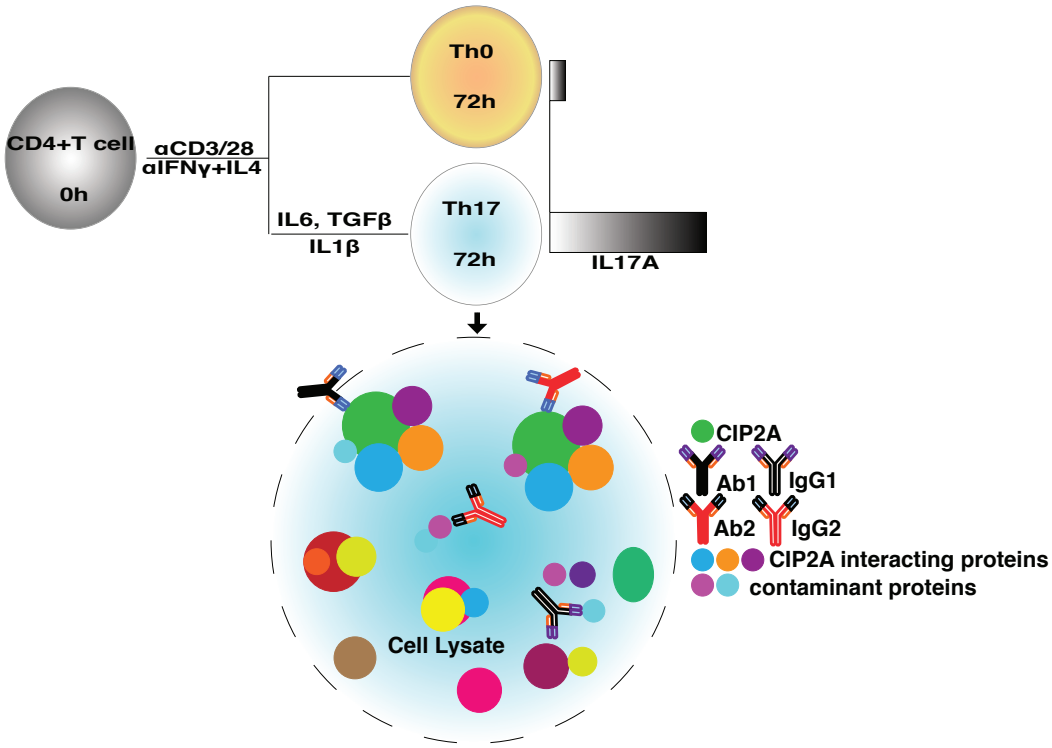


| Protein | Spectral Intensity (Ab) | Spectral Intensity (IgG) | Interactome |
|---|---|---|---|
| Protein A | | | Interactor |
| Protein B | | | Interactor |
| Protein C | | | Contaminent |
| Protien D | | | Contaminent |

+

0

**Supplementary Figure S2** (Related to Figure 2)

**A**

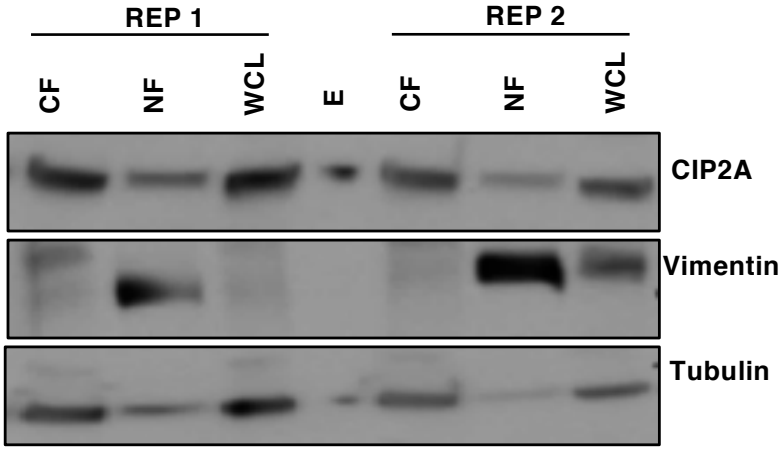

**Supplementary Figure S3** (Related to Figure 3)

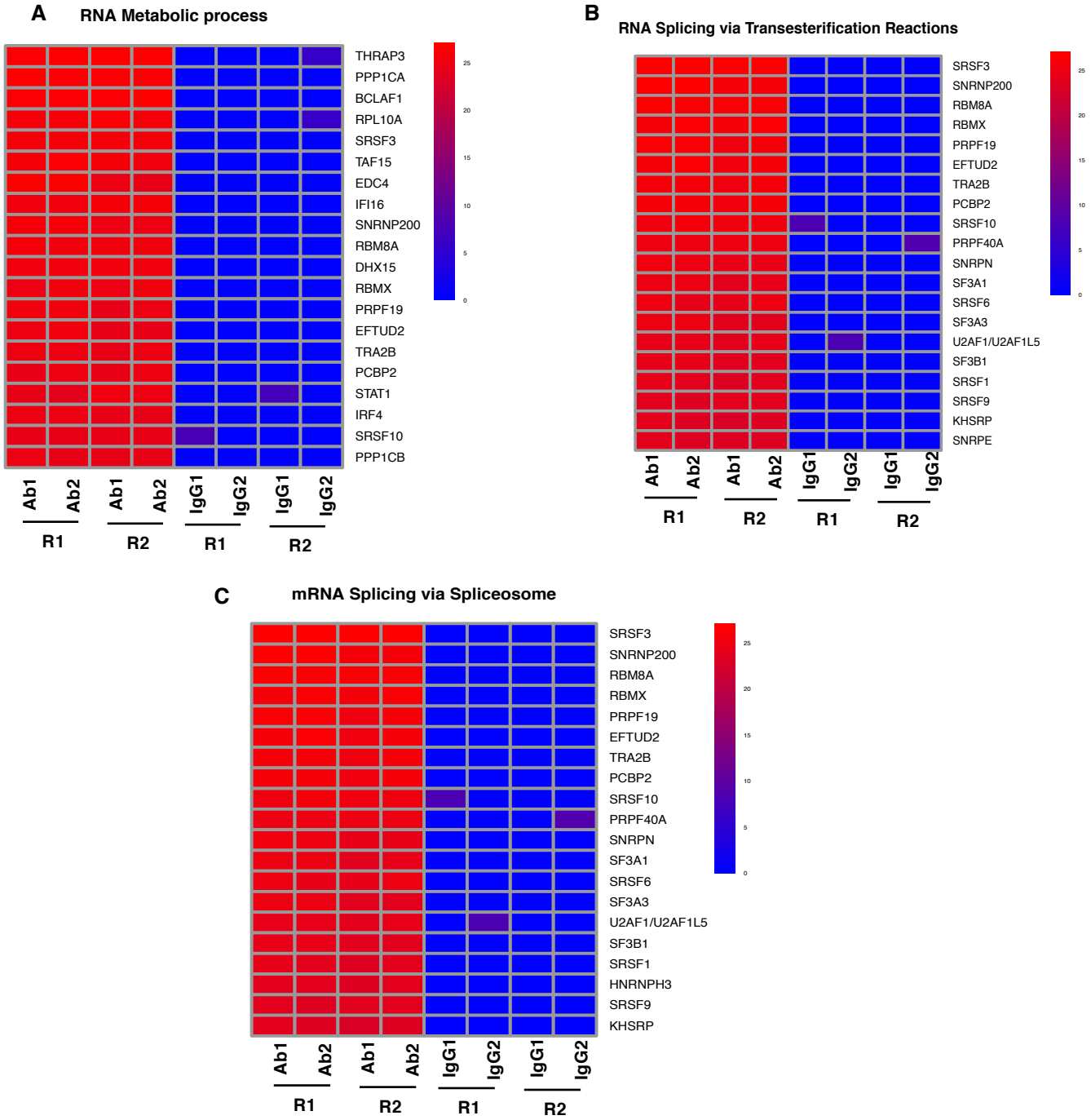

**Supplementary Figure S4** (Related to Figure 4)

**A**

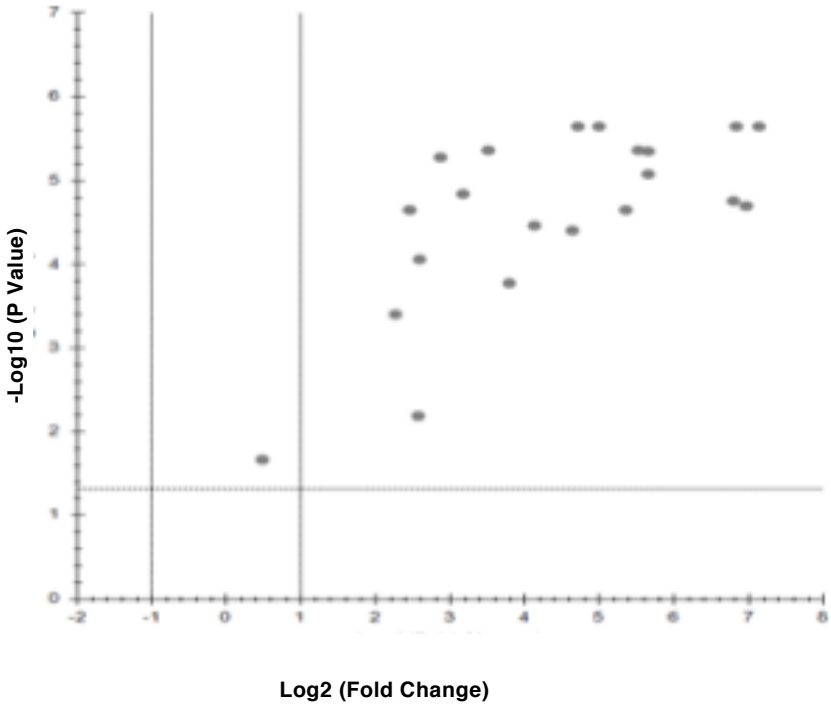
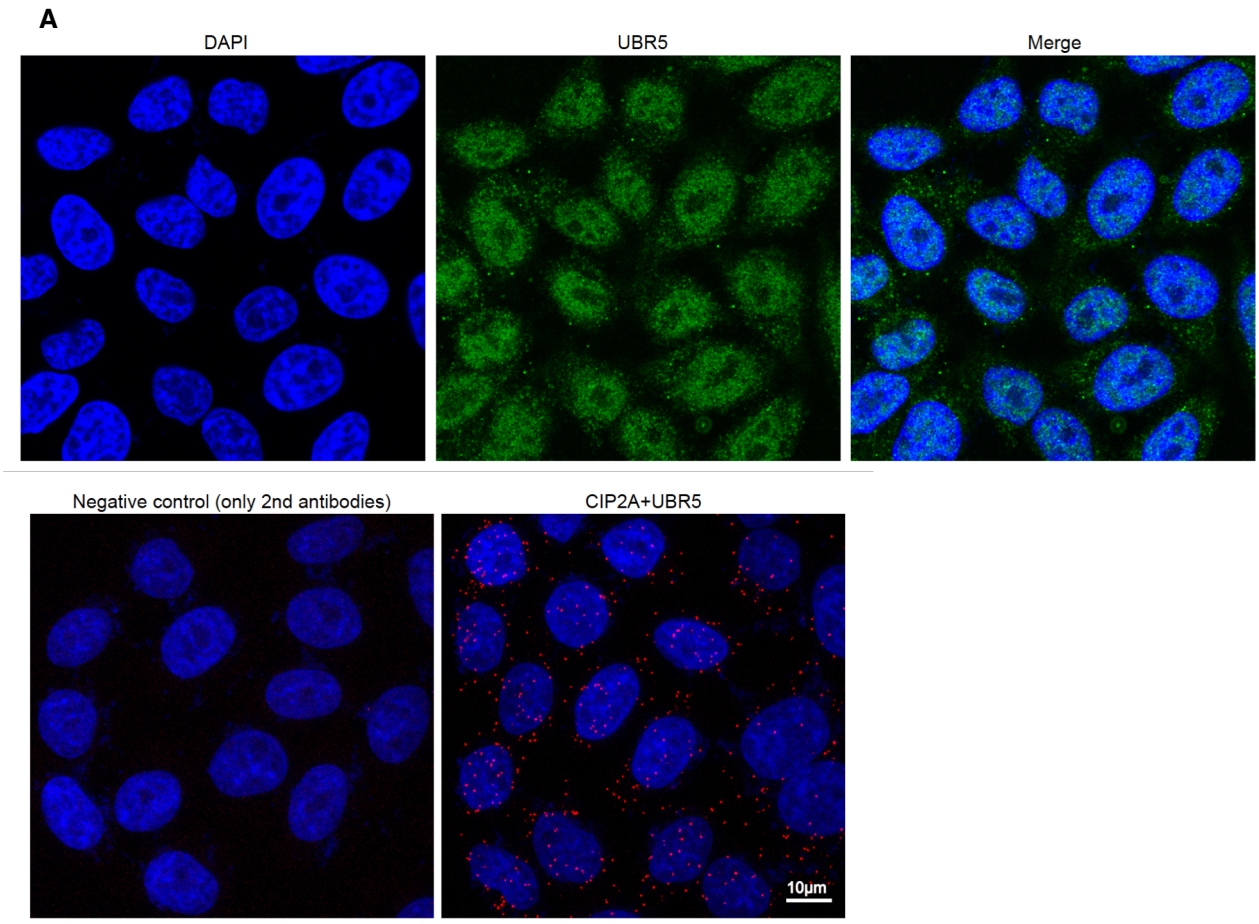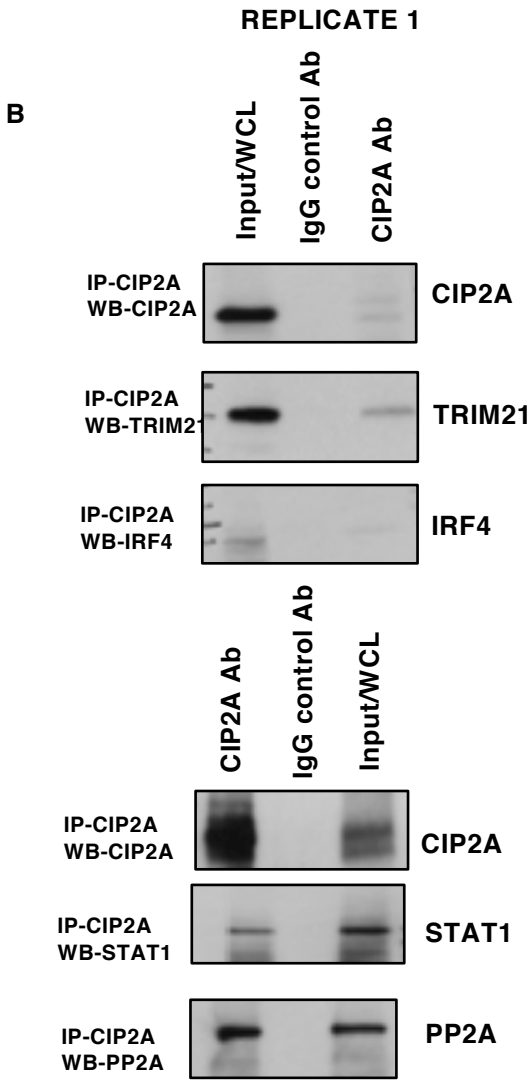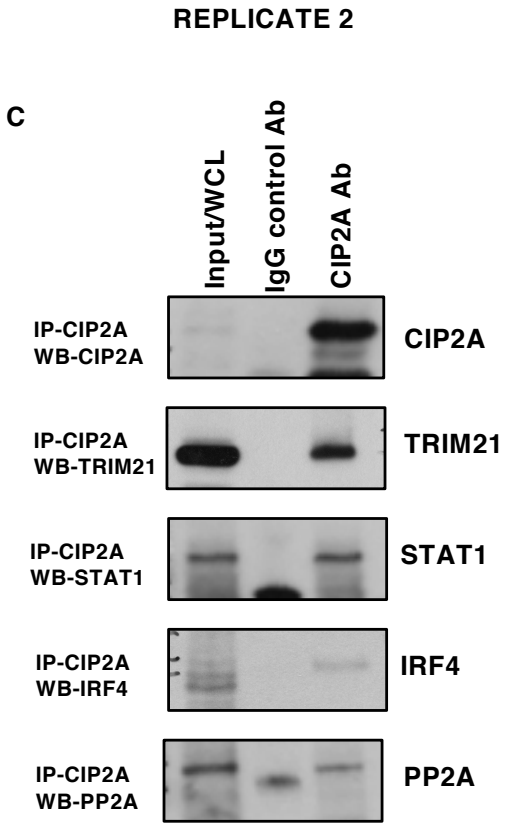
**Supplementary Figure S5** (Related to Figure 5)